JOURNAL OF CELLULAR PHYSIOLOGY 204:896–900 (2005)

Dominant Expression of Androgen Receptors and Their Functional Regulation of Organic Anion Transporter 3 in Rat Brain Capillary Endothelial Cells; Comparison of Gene Expression Between the Blood–Brain and -Retinal Barriers

SUMIO OHTSUKI,[1,2,3] MASATOSHI TOMI,[3,4] TOSHIO HATA,[1] YOKO NAGAI,[1] SATOKO HORI,[1,2,3] SHINOBU MORI,[1] KEN-ICHI HOSOYA,[3,4] AND TETSUYA TERASAKI[1,2,3]*

[1]*Department of Molecular Biopharmacy and Genetics, Graduate School of Pharmaceutical Sciences, Sendai, Japan*
[2]*New Industry Creation Hatchery Center, Tohoku University, Sendai, Japan*
[3]*CREST and SORST of the Japan Science and Technology Agency (JST), Japan*
[4]*Faculty of Pharmaceutical Sciences, Toyama Medical and Pharmaceutical University, Toyama, Japan*

Brain and retinal capillary endothelial cells (BCECs and RCECs, respectively) exhibit a barrier structure and function. Comparison of gene expression in these cells could clarify the selective function of each barrier. The purpose of this study was to identify the genes selectively expressed at the blood–brain barrier (BBB) and to clarify the function of the selective gene, androgen receptor (AR). Gene expression was compared by a differential display using conditionally immortalized rat BCECs and RCECs (TR-BBB and TR-iBRB, respectively). A total of 12 gene fragments were identified as the selective genes dominantly expressed in TR-BBB cells. The most selective fragment in TR-BBB cells had the highest homology with the 3′-UTR of human and mouse AR. Rat AR mRNA was detected in TR-BBB cells and the brain capillary rich fraction, but not in TR-iBRB cells. Expression of organic anion transporter 3 (OAT3) mRNA in TR-BBB cells was induced by treatment with dihydrotestosterone (DHT), an AR ligand, and this induction was suppressed by flutamide. Moreover, uptake of benzylpenicillin by TR-BBB cells was also induced by DHT treatment. In contrast, OAT3 mRNA expression in TR-iBRB cells was not affected by DHT treatment. The brain-to-blood efflux rate of benzylpenicillin was not affected by gender. These results suggest that AR is involved in the functional regulation of OAT3 at the BBB, but not at the inner blood-retinal barrier (iBRB), and this regulation is not affected by gender. The BBB function will be affected by the androgen levels in the brain and/or plasma via AR. J. Cell. Physiol. 204: 896–900, 2005. © 2005 Wiley-Liss, Inc.

The blood–brain barrier (BBB) is formed by brain capillary endothelial cells (BCECs) with tight junctions. The BBB expresses various transporters, which act to support and protect the central nervous system (CNS) by supplying nutrients to the brain and excreting metabolites, toxins, and drugs from the brain to blood. Compared with peripheral capillary endothelial cells, BCECs express a variety of unique molecules, such as transporters, receptors, and tight junction proteins (Hosoya et al., 2002), however the molecular mechanisms that induce and maintain the BBB functions in BCECs are still poorly understood.

Gene comparison is one of the most effective strategies for identifying the molecules that are selectively expressed at the BCECs and play unique roles at the BBB. Li and co-workers have reported gene subtraction between rat BCECs, liver and kidney (Li et al., 2002). However, the gene expression in different tissues is too different to allow identification of the molecules controlling the unique functions of the BBB, since the cells in these tissues are a mixture of different type of cells with totally different functions. Therefore, gene comparison should be performed between endothelial cells forming the barrier system in different tissues.

RCECs form the inner blood–retinal barrier (iBRB) by connect with tight junctions as well as BCECs (Cunha-Vaz, 1976). We recently established conditionally immortalized rat BCECs and RCECs (TR-BBB and TR-iBRB, respectively) from transgenic rats harboring a temperature-sensitive SV 40 large T-antigen gene (Hosoya et al., 2000, 2001). TR-BBB and TR-iBRB cells possess endothelial markers and express GLUT1 and P-glycoprotein (Hosoya et al., 2000, 2001), which are expressed at the BBB and inner BRB in vivo as shown by immunohistochemical analysis (Tsuji et al., 1992; Holash and Stewart, 1993; Kumagai, 1999). Thus, TR-BBB and TR-iBRB cells maintain certain in vivo functions, and are a suitable in vitro model for the BBB and iBRB, respectively (Terasaki et al., 2003).

Contract grant sponsor: Japan Society for the Promotion of Science (for Scientific Research and a 21st Century Center of Excellence (COE) Program); Contract grant sponsor: Industrial Technology Research Grant Program of the New Energy and the Industrial Technology Development Organization (NEDO) of Japan.

*Correspondence to: Tetsuya Terasaki, Department of Molecular Biopharmacy and Genetics, Graduate School of Pharmaceutical Sciences, Tohoku University, Aoba, Aramaki, Aoba-ku, Sendai 980-8578, Japan. E-mail: terasaki@mail.pharm.tohoku.ac.jp

Received 12 October 2004; Accepted 4 January 2005

DOI: 10.1002/jcp.20352

The purpose of the present study was to identify selectively expressed genes at the BBB by mRNA differential display analysis of TR-BBB and TR-iBRB cells. The differential display analysis has shown that the androgen receptor (AR) gene is predominantly expressed in TR-BBB cells, and the regulation of transport by AR at the BBB was examined using TR-BBB cells.

MATERIALS AND METHODS

Cell culture

TR-BBB11, TR-BBB13, TR-iBRB2, and TR-iBRB9 cells were established and characterized as described previously (Hosoya et al., 2000, 2001). Cells were seeded onto rat tail collagen type I-coat tissue culture dishes (Becton Dickinson, Bedford, MA). The cells were then cultured in Dulbecco's modified Eagle's medium supplemented with 10% fetal bovine serum (Moregate, Bulimbra, Australia) and 15 μg/l endothelial cell growth factor (Roche Diagnostics, Mannheim, Germany) at 33°C in a humidified atmosphere of 5% CO_2/air. For treatment with DHT or flutamide, the cells were cultured at 33°C with the above medium containing 10 nM DHT (Wako Pure Chemicals, Osaka, Japan) and 0.1% ethanol, or with 10 nM DHT, 1 μM flutamide (Sigma, St. Louis, MO), and 0.1% ethanol. As a control, culture medium containing 0.1% ethanol was used.

mRNA differential display analysis

Differential display was performed using the rhodamine version of a fluorescence differential display kit (Takara, Shiga, Japan) as described previously (Tomi et al., 2004). Briefly, total RNA was prepared from the culture cells using TRIzol reagent (Invitrogen, Carlsbad, CA). After DNase I treatment, RNA was reverse transcribed with a rhodamine labeled arbitrary anchored oligo dT primer. The resulting cDNA was PCR-amplified using the rhodamine labeled arbitrary anchored oligo dT primer and an arbitrary decamer. PCR products were loaded on to 6% polyacrylamide gels, and DNA bands were visualized using a fluorescent image analyzer (FLA3000; Fujifilm, Tokyo, Japan). DNA bands differentially displayed between TR-BBB and TR-iBRB cells were excised from the gel. The eluted DNA was reamplified using the same primer set and PCR conditions. Reamplified PCR products were run on 3% agarose gel containing H.A.-Yellow (Takara) and visualized using the fluorescent image analyzer. The DNA was cloned into a plasmid (pBluescript II SK+; Stratagene, La Jolla, CA), and sequenced using a DNA sequencer (CEQ2000XL; Beckman Coulter, Fullerton, CA). Similarities with other sequences in the GenBank were examined using the BLAST program at the National Center for Biotechnology Information (Bethesda, MD).

RT-PCR analysis

Isolation of the rat brain capillary-rich fraction was performed as described previously (Hosoya et al., 2000). Briefly, cerebrum excised from rats was dissected into pieces, and homogenized in phosphate-buffered saline (PBS). Homogenate was added to the same volume of 32% dextran solution, and then centrifuged (4,500*g*, 20 min, 4°C). The resulting pellets were washed in PBS to obtain the enriched capillary fraction. Total RNA was prepared from the brain capillary-rich fraction using TRIzol reagent (Invitrogen). Reverse-transcription was performed with oligo dT primer. The sequences of the specific primers for AR were as follows: sense, GGTATCCTGGTGGAGTTGTGAACA and antisense, TCACTGTGTGTGGAAATAGATGGGC for rat AR (NM012502; position 2477–3702). PCR was conducted through 35 cycles of 94°C for 30 sec, 55°C for 30 sec, and 72°C for 1 min. The RT-PCR products were separated by electrophoresis on agarose gel. All PCR products were subcloned and sequenced using a DNA sequencer.

Quantitative real-time PCR analysis

Quantitative real-time PCR was performed as described previously (Tomi et al., 2004). Briefly, single-strand cDNA was synthesized from total RNA (1 μg) by reverse transcription using oligo dT primer. According to the manufacturer's protocol, quantitative real-time PCR was performed using an ABI PRISM 7700 sequence detector system (PE-Applied Biosystems) with a 2× SYBR Green PCR master mix (PE-Applied Biosystems), reverse transcribed cDNA, and gene-specific primers. To quantify the amount of target mRNA in the samples, a standard curve was prepared for each run using the plasmid containing the target gene. The mRNA content of organic anion transporter 3 (OAT3) was quantitated within the range of standards, and was standardized by the amount of glyceraldehyde-3-phosphate dehydrogenase (GAPDH). The primer set and amplify condition for AR were the same as that used in RT-PCR analysis. The sequences of the specific primers were as follows: sense, ATCTCATCAACATCTATTGGGT and antisense, CAGAGAGAGACAGAAGGTCA for rat OAT3 (AB017446; position 748–1119); sense, 5′-TGATGACATCAAGAAGGTGGTGAAG-3′ and antisense, 5′-TCCTTGGAGGCCATGTAGGCCAT-3′ for GAPDH (XM217111; position 830–1069). PCR was conducted through 40 cycles of 94°C for 30 sec, 60°C for 1 min, and 72°C for 1 min. The statistical significance of differences among means of several groups was determined by one-way analysis of variance (ANOVA) followed by the modified Fisher's least squares difference method.

Cell uptake study

TR-BBB13 cells (1×10^5 cells/cm^2) were washed with prewarmed uptake buffer A (135 mM NaCl, 3 mM KCl, 1.4 mM $CaCl_2$, 1.2 mM $MgSO_4$, 0.4 mM K_2HPO_4, 10 mM D-glucose, and 10 mM HEPES, pH 7.4, 290 ± 15 mOsm/kg) at 37°C. The uptake study was initiated at 37°C by applying 200 μl uptake buffer A containing 4.0 μCi [^{3}H]benzylpenicillin (21.0 Ci/mmol, Amersham Biotech, Uppsala, Sweden) and 1.0 μCi [^{14}C]inulin (2.64 Ci/mmol, NEN Life Science, Boston, MA) to estimate the volume of adherent water. After a predetermined interval, cells were washed with ice-cold uptake buffer A and solubilized. Radioactivity was measured in a liquid scintillation counter (LS6500, Beckman-Coulter, Fullerton, CA) and the protein content was determined using a kit (DC, Bio-Rad, Hercules, CA) with bovine serum albumin as a standard. The uptake of [^{3}H]benzylpenicillin was expressed as the cell-to-medium (cell/medium) ratio using the following equation:

$$\text{Cell/medium ratio} = ([^3\text{H}]\ \text{dpm per cell protein (mg)})/([^3\text{H}]\ \text{dpm/μl medium}) - ([^{14}\text{C}]\ \text{dpm per cell protein (mg)})/([^{14}\text{C}]\ \text{dpm/μl medium}).$$

Brain efflux index (BEI) method

The BEI method was performed by the intracerebral microinjection technique as described previously (Kakee et al., 1996). In brief, Wistar rats were anesthetized by intramuscular injection of ketamine-xylazine (1.22 mg xylazine and 125 mg ketamine per kg). Then a freshly prepared solution (0.50 μl), containing 320 nCi [^{14}H]benzylpenicillin and 16 nCi [^{14}C]inulin in an extracellular fluid buffer (122 mM NaCl, 25 mM $NaHCO_3$, 3 mM KCl, 1.4 mM $CaCl_2$, 1.2 mM $MgSO_4$, 0.4 mM K_2HPO_4, 10 mM D-glucose, and 10 mM HEPES, pH 7.4), was administered into the Parietal Cortex Area 2 region over a period of 1 min. At designated times (2, 20, and 40 min), the whole brain was removed and the left cerebrum, right cerebrum, and cerebellum were isolated. Brain samples were solubilized and mixed with Hionic-fluor (Packard, Meriden, CT). The radioactivity remaining in the brain was measured in a liquid scintillation counter. The percentage of substrate remaining in the ipsilateral cerebrum (100-BEI) was determined from following equation:

$$\text{100-BEI (\%)} = [(\text{amount of test substrate in the brain})/(\text{amount of reference in the brain})]/[(\text{concentration of test substrate injected})/(\text{concentration of reference injected})] \times 100.$$

The apparent brain efflux rate constant (k_{eff}) across the BBB was estimated from the slope given by fitting a semilogarithmic plot of (100-BEI), that is, the concentration remaining in the

TABLE 1. Genes dominantly expressed in TR-BBB cells

No.	Length (bp)	mRNA ratio	Highest homology genes	Identity
1	287	1,730	Mouse androgen receptor, 3'-UTR	91/91 (100%)
2	389	16.9	Mouse clone RP23-443D3 (Chr2)	80/88 (90%)
3	95	8.08	Mouse clone RP23-47J12 (Chr11)	70/75 (93%)
4	375	6.88	Mouse clone RP23-60i12 (Chr2)	113/133 (84%)
5	92	4.52	Mouse hypothetical protein LOC217831	81/86 (94%)
6	136	3.32	Rat BAC CH230-9H16	57/61 (93%)
7	194	2.99	Rat hypothetical protein LOC309523	152/153 (99%)
8	300	2.96	Rat BAC CH230-24G20	298/298 (100%)
9	204	2.75	Mouse clone IMAGE:5354131	163/181 (90%)
10	391	2.47	Mouse clone RP23-445E3 (Chr4)	134/165 (81%)
11	284	2.43	Mouse cDNA clone:6030408G03	195/220 (88%)
12	112	2.26	Mouse clone RP24-75F14 (Chr1)	98/111 (88%)

The mRNA ratio is the ratio of the mRNA level in TR-BBB cells to that in TR-iBRB cells normalized by the mRNA level of GAPDH. Identity indicates the number of identical nucleotide versus the number of nucleotide in the identical region.

ipsilateral cerebrum versus time, using nonlinear least-squares regression analysis.

RESULTS

Differential display between TR-BBB and TR-iBRB cells

The differential display analysis of TR-BBB11, TR-BBB13, TR-iBRB2, and TR-iBRB9 cells showed a number of DNA bands selectively expressed in TR-BBB cells. The DNA bands of 100 ~ 450 bp were cloned and sequenced. Quantitative real-time PCR using specific primers for each clone was performed to confirm the reproducibility. As a result of these analyses, 12 clones were identified and found to be expressed to a greater extent in TR-BBB cells than in TR-iBRB cells (Table 1). Clone 1 of 287 bp, which was expressed 1730-fold more intensely in TR-BBB cells than in TR-iBRB cells, exhibited the largest difference in mRNA expression level of the 12 clones. A portion of the sequence of clone 1 exhibited 100% and 99 % nucleotide identity with the 3'-UTR of the mouse and human AR (99/99 and 120/121), respectively.

Dominant expression of AR in rat BCECs

The expression of rat AR mRNA was examined by RT-PCR analysis amplifying the coding region of rat AR (Fig. 1). A band was detected in TR-BBB11, TR-BBB13 cells, and brain capillary-rich fraction at the expected size, while no band was detected in TR-iBRB2 and TR-iBRB9 cells. The expression of AR mRNA was quantified by means of real-time RT-PCR standardized by that of GAPDH mRNA, and the expression of AR mRNA in TR-BBB cells is 3,400-fold higher than that in TR-iBRB cells. The sequence of the amplified product was identical to that of rat AR.

Induction of OAT3 expression by AR

OAT3 is a transporter expressed at the BBB, and its expression in males has been reported to be greater than that in females as far as the liver and kidney are concerned (Kobayashi et al., 2002; Ljubojevic et al., 2004). Therefore, the regulation of OAT3 mRNA expression by AR was investigated (Fig. 2). The mRNA expression of AR was normalized by that of GAPDH, and the expression levels of GAPDH mRNA in the cells varied less than twofold in this experiment (data not shown). TR-BBB13 cells were treated with dihydrotestosterone (DHT), an AR ligand. At 9 and 12 h after treatment, OAT3 mRNA expression was induced 1.65- and 1.95-fold, respectively, compared with the untreated cells. This induction was almost completely suppressed by flutamide, an AR inhibitor. In contrast, no induction of OAT3 mRNA by DHT was detected in TR-iBRB2 cells.

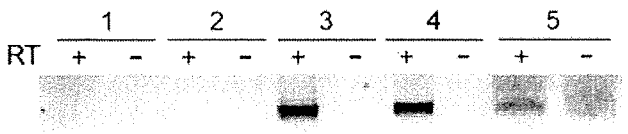

Fig. 1. Selective mRNA expression of rat AR in TR-BBB cells and the brain capillary-rich fraction. An amplified band was detected at 1018 bp. (1) TR-iBRB2 cells; (2) TR-iBRB9 cells; (3) TR-BBB11 cells; (4) TR-BBB13 cells; (5) rat brain capillary-rich fraction. Reactions were performed against total RNA with (+) or without (−) reverse transcription (RT).

Induction of OAT3 function by AR

The transport function of OAT3 was evaluated by cellular uptake using [^{3}H]benzylpenicillin, a specific substrate for OAT3. [^{3}H]Benzylpenicillin uptake by TR-BBB13 cells increased linearly for at least 10 min (Fig. 3), and so the transport function of OAT3 was evaluated at 5 min.

After DHT treatment for less than 24 h, no difference in [^{3}H]benzylpenicillin uptake was detected between DHT-treated and control cells (Fig. 4). After treatment for 36 and 72 h, the uptake increased by 1.56- and 1.67-fold compared with control cells, respectively (Fig. 4). This result suggests that the transport function of OAT3 is induced by DHT.

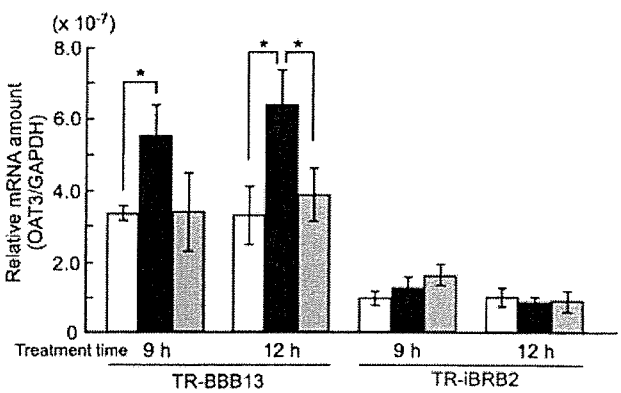

Fig. 2. Effect of DHT and flutamide on mRNA levels of rat OAT3 in TR-BBB13 and TR-iBRB2 cells. TR-BBB13 and TR-iBRB2 cells were treated with culture medium containing either 10 nM DHT (■) or 10nM DHT and 1 μM flutamide (▨), or control medium (□). mRNA levels of OAT3 were normalized by the mRNA levels of GAPDH. Each bar represents the mean ± SEM (n = 3–6). *$P < 0.05$, significant difference.

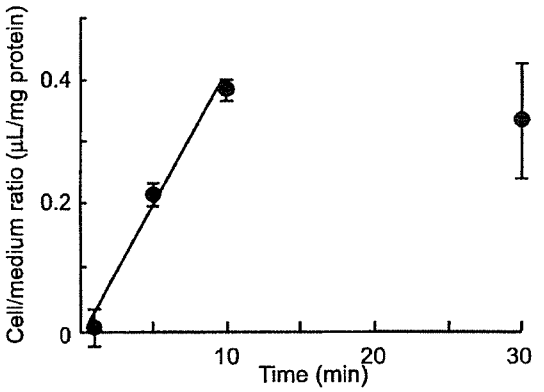

Fig. 3. Uptake of [^{3}H]benzylpenicillin by TR-BBB13 cells. The uptake of [^{3}H]benzylpenicillin was measured at 1, 5, 10, and 30 min. The uptake was expressed as the cell-to-medium (cell/medium) ratio. The initial uptake, which was estimated by least-squares regression, is indicated as a line. The initial uptake rate was calculated to be 4.21×10^{-2} μl/(mg protein × min). Each point represents the mean ± SEM (n = 4).

Effect of gender on OAT3-mediated efflux transport at the BBB

To investigate the effect of gender on OAT3 function at the in vivo BBB, the brain-to-blood efflux transport of [^{3}H]benzylpenicillin was examined by the BEI method. The efflux rates of male and female animals were found to be $5.57 \times 10^{-2} \pm 0.52 \times 10^{-2}$/min and $6.46 \times 10^{-2} \pm 0.46 \times 10^{-2}$/min (mean ± SEM, n = 3), respectively, and there was no significant difference between the efflux rate of males and females.

DISCUSSION

In this study, 12 gene clones were identified as highly expressed genes in rat BCECs (TR-BBB cells) compared with RCECs (TR-iBRB cells) by mRNA differential display analysis (Table 1). Using these culture cells overcame the problems posed by contamination by non-endothelial cells and the limited size of the organs. In addition, TR-BBB and TR-iBRB cells were established from the same strain of male transgenic rat, harboring temperature sensitive SV40 large T antigen gene, of the same age by using a similar procedure, which did not involve gene transfection (Terasaki et al., 2003). Therefore, the difference in expressed genes between these cell lines did indeed reflect the difference between the BBB and iBRB in vivo.

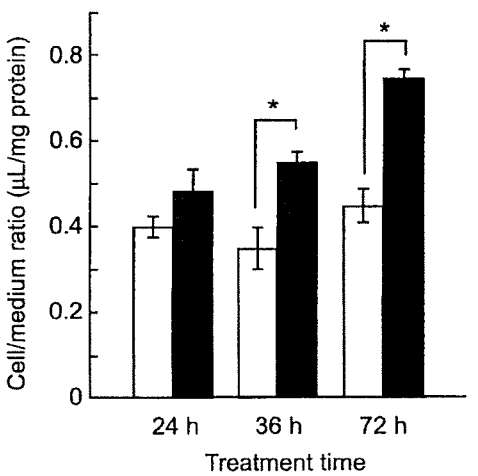

Fig. 4. Effect of DHT on the uptake of benzylpenicillin by TR-BBB cells. TR-BBB cells were cultured in the presence (■) or absence (control, □) of 10 nM DHT. The uptake was measured at 5 min. Each bar represents the mean ± SEM (n = 4). *$P < 0.05$, significantly different from control.

The function of the identified BBB dominant genes, except clone 1, is unknown, since these gene fragments have the highest homology with functionally unknown genes (Table 1). The BBB dominant expression of these genes might provide helpful information for further studies of their gene function. The differential display using TR-BBB and TR-iBRB cells could also be used to identify the iBRB dominant gene. We have already reported that M-cadherin, GATA-binding protein-3, and cytosolic branched chain amino transferase are more abundantly expressed in TR-iBRB cells than TR-BBB cells and may be involved in unique functions at the iBRB (Tomi et al., 2004).

AR is a nuclear receptor regulating gene expression by binding to androgens (Santos et al., 2004). The most selective gene fragment in TR-BBB cells has a high degree of homology with the 3′-UTR of mouse and human AR. The nucleotide sequence of rat AR cDNA including 3′-UTR has been reported (Chang et al., 1988), whereas a sequence similar to that of the identified gene fragment was not found in the reported rat AR cDNA. Human AR has been reported to have splicing variants, which have different lengths of 3′-UTR (Faber et al., 1991). Therefore, the reported rat AR cDNA would be a splicing variant lacking the region of the identified fragment. Following RT-PCR analysis of the coding region, AR mRNA was found to be expressed in TR-BBB cells and the brain capillary rich-fraction, but not in TR-iBRB cells (Fig. 1). This result suggests selective mRNA expression of AR at the BBB.

Gene and functional induction by DHT, an AR ligand, was detected in TR-BBB13 cells, and this induction was suppressed by flutamide (Fig. 2). Although estrogens, which are produced from androgens by aromatase, are able to induce gene expression by interaction with estrogen receptors (Allolio and Arlt, 2002), the inhibition of flutamide indicates that the induction of OAT3 expression and function by DHT resulted from an interaction between DHT and AR. In contrast, no gene induction by DHT was detected in TR-iBRB cells (Fig. 2). These results suggest that an AR-mediating gene regulation exists at the BBB but not at the iBRB. In the non-treated conditions, OAT3 expression in TR-BBB cells is greater than that in TR-iBRB cells (3.3-fold at 12 h treatment). This suggests that the OAT3 was basally induced in TR-BBB cells.

Gene induction of OAT3 was detected after 9 h of DHT treatment, while significant functional induction of OAT3 was detected after 36 h of the treatment. The functional delay of transporters has also been detected in the induction of system A in TR-BBB cells under hypertonic conditions (Takanaga et al., 2002). This functional delay could be attributed to the transcription from mRNA, molecular modification, and translocation to the plasma membrane.

The present study is the first demonstration of the AR-mediated regulation of OAT3 function at the BBB. Male dominant expression of OAT3 has been reported in rat liver and kidney (Kobayashi et al., 2002; Ljubojevic et al., 2004). These reports have also shown that OAT3 expression in the liver and kidney was reduced in castrated male rats, and this reduction was reversed by testosterone treatment, but not by estradiol treatment. Searching the upstream region of rat OAT3, the sequence, which is similar to the high-affinity AR

specific androgen response element in rat probasin promoter (5′-GGTTCTtgcAGTACT-3′) (Claessens et al., 1996), is located 1 kbp upstream from the potent transcription start site (−1126: 5′-GGTAATcctAGTACT-3′: −1112). Therefore, it is conceivable that the induction of OAT3 gene is mediated by the interaction of AR and the *cis*-response element on the OAT3 promoter.

The BCECs face the circulating blood and also the brain parenchyma. Sex hormones exist in the brain, and the brain level of dehydroepiandrosterone (DHEA) is about fourfold higher than that in plasma (Corpechot et al., 1981; Hojo et al., 2004). Therefore, it is likely that androgen signals from the brain control the AR mediating gene regulation rather than those from the circulating blood. Indeed, no gender difference was detected in the brain-to-blood efflux rate of benzylpenicillin, an OAT3 selective substrate, in adult rats. The possibility that the contribution of other regulatory mechanism(s) also plays a role in maintaining OAT3 function at the BBB cannot be ruled out or that the limiting process in the efflux transport of benzylpenicillin is luminal efflux transport and not abluminal uptake by OAT3, the dominant regulation from the brain side agrees with the physiological function of OAT3 at the BBB. Because OAT3 is the transporter responsible for the brain-to-blood efflux of dopamine metabolites, such as homovanillic acid, uremic toxins, and drugs (Ohtsuki et al., 2002, 2004; Mori et al., 2003, 2004). If OAT3 expression is influenced by the plasma levels of androgens, which exhibit gender and diurnal variations, the BBB will be unable to maintain a constant CNS milieu.

In conclusion, the present study describes a comparison of gene expression between the rat BBB and iBRB, and the identification of 12 BBB dominant genes. AR, which is the most selective BBB gene, regulates the expression and function of OAT3 at the BBB. These results suggest that the comparison of gene expression is one of the most effective strategies for identifying novel barrier functions and regulation systems. In addition, the further analysis of the genes regulated by AR at the BBB will play an important role in increasing our understanding of the physiological function of the AR at the BBB and the effects of sex hormones on BBB functions under physiological and pathological conditions.

ACKNOWLEDGMENTS

We thank Ms. N. Funayama for secretarial assistance.

LITERATURE CITED

Allolio B, Arlt W. 2002. DHEA treatment: Myth or reality? Trends Endocrinol Metab 13(7):288–294.

Chang CS, Kokontis J, Liao ST. 1988. Structural analysis of complementary DNA and amino acid sequences of human and rat androgen receptors. Proc Natl Acad Sci USA 85(19):7211–7215.

Claessens F, Alen P, Devos A, Peeters B, Verhoeven G, Rombauts W. 1996. The androgen-specific probasin response element 2 interacts differentially with androgen and glucocorticoid receptors. J Biol Chem 271(32):19013–19016.

Corpechot C, Robel P, Axelson M, Sjovall J, Baulieu EE. 1981. Characterization and measurement of dehydroepiandrosterone sulfate in rat brain. Proc Natl Acad Sci USA 78(8):4704–4707.

Cunha-Vaz JG. 1976. The blood-retinal barriers. Doc Ophthalmol 41(2):287–327.

Faber PW, van Rooij HC, van der Korput HA, Baarends WM, Brinkmann AO, Grootegoed JA, Trapman J. 1991. Characterization of the human androgen receptor transcription unit. J Biol Chem 266(17):10743–10749.

Hojo Y, Hattori TA, Enami T, Furukawa A, Suzuki K, Ishii HT, Mukai H, Morrison JH, Janssen WG, Kominami S, Harada N, Kimoto T, Kawato S. 2004. Adult male rat hippocampus synthesizes estradiol from pregnenolone by cytochromes P45017alpha and P450 aromatase localized in neurons. Proc Natl Acad Sci USA 101(3):865–870.

Holash JA, Stewart PA. 1993. The relationship of astrocyte-like cells to the vessels that contribute to the blood-ocular barriers. Brain Res 629(2):218–224.

Hosoya K, Takashima T, Tetsuka K, Nagura T, Ohtsuki S, Takanaga H, Ueda M, Yanai N, Obinata M, Terasaki T. 2000. mRNA expression and transport characterization of conditionally immortalized rat brain capillary endothelial cell lines; a new in vitro BBB model for drug targeting. J Drug Target 8(6):357–370.

Hosoya K, Tomi M, Ohtsuki S, Takanaga H, Ueda M, Yanai N, Obinata M, Terasaki T. 2001. Conditionally immortalized retinal capillary endothelial cell lines (TR-iBRB) expressing differentiated endothelial cell functions derived from a transgenic rat. Exp Eye Res 72(2):163–172.

Hosoya K, Ohtsuki S, Terasaki T. 2002. Recent advances in the brain-to-blood efflux transport across the blood-brain barrier. Int J Pharm 248(1–2):15–29.

Kakee A, Terasaki T, Sugiyama Y. 1996. Brain efflux index as a novel method of analyzing efflux transport at the blood-brain barrier. J Pharmacol Exp Ther 277(3):1550–1559.

Kobayashi Y, Hirokawa N, Ohshiro N, Sekine T, Sasaki T, Tokuyama S, Endou H, Yamamoto T. 2002. Differential gene expression of organic anion transporters in male and female rats. Biochem Biophys Res Commun 290(1):482–487.

Kumagai AK. 1999. Glucose transport in brain and retina: Implications in the management and complications of diabetes. Diabetes Metab Res Rev 15(4):261–273.

Li JY, Boado RJ, Pardridge WM. 2002. Rat blood-brain barrier genomics II. J Cereb Blood Flow Metab 22(11):1319–1326.

Ljubojevic M, Herak-Kramberger CM, Hagos Y, Bahn A, Endou H, Burckhardt G, Sabolic I. 2004. Rat renal cortical OAT1 and OAT3 exhibit gender differences determined by both androgen stimulation and estrogen inhibition. Am J Physiol Renal Physiol 287(1):F124–F138.

Mori S, Takanaga H, Ohtsuki S, Deguchi T, Kang YS, Hosoya K, Terasaki T. 2003. Rat organic anion transporter 3 (rOAT3) is responsible for brain-to-blood efflux of homovanillic acid at the abluminal membrane of brain capillary endothelial cells. J Cereb Blood Flow Metab 23(4):432–440.

Mori S, Ohtsuki S, Takanaga H, Kikkawa T, Kang YS, Terasaki T. 2004. Organic anion transporter 3 is involved in the brain-to-blood efflux transport of thiopurine nucleobase analogs. J Neurochem 90(4):931–941.

Ohtsuki S, Asaba H, Takanaga H, Deguchi T, Hosoya K, Otagiri M, Terasaki T. 2002. Role of blood-brain barrier organic anion transporter 3 (OAT3) in the efflux of indoxyl sulfate, a uremic toxin: Its involvement in neurotransmitter metabolite clearance from the brain. J Neurochem 83(1):57–66.

Ohtsuki S, Kikkawa T, Mori S, Hori S, Takanaga H, Otagiri M, Terasaki T. 2004. Mouse reduced in osteosclerosis transporter functions as an organic anion transporter 3 and is localized at abluminal membrane of blood-brain barrier. J Pharmacol Exp Ther 309(3):1273–1281.

Santos AF, Huang H, Tindall DJ. 2004. The androgen receptor: A potential target for therapy of prostate cancer. Steroids 69(2):79–85.

Takanaga H, Tokuda N, Ohtsuki S, Hosoya K, Terasaki T. 2002. ATA2 is predominantly expressed as system A at the blood-brain barrier and acts as brain-to-blood efflux transport for L-proline. Mol Pharmacol 61(6):1289–1296.

Terasaki T, Ohtsuki S, Hori S, Takanaga H, Nakashima E, Hosoya K. 2003. New approaches to in vitro models of blood-brain barrier drug transport. Drug Discov Today 8(20):944–954.

Tomi M, Abukawa H, Nagai Y, Hata T, Takanaga H, Ohtsuki S, Terasaki T, Hosoya K. 2004. Retinal selectivity of gene expression in rat retinal versus brain capillary endothelial cell lines by differential display analysis. Mol Vis 10:537–543.

Tsuji A, Terasaki T, Takabatake Y, Tenda Y, Tamai I, Yamashima T, Moritani S, Tsuruo T, Yamashita J. 1992. P-glycoprotein as the drug efflux pump in primary cultured bovine brain capillary endothelial cells. Life Sci 51(18):1427–1437.

Impact of the Liver-Specific Expression of SHIP2 (SH2-Containing Inositol 5′-Phosphatase 2) on Insulin Signaling and Glucose Metabolism in Mice

Kazuhito Fukui,[1] Tsutomu Wada,[1] Syota Kagawa,[2] Kiyofumi Nagira,[1] Mariko Ikubo,[1] Hajime Ishihara,[3] Masashi Kobayashi,[1] and Toshiyasu Sasaoka[2]

We investigated the role of hepatic SH2-containing inositol 5′-phosphatase 2 (SHIP2) in glucose metabolism in mice. Adenoviral vectors encoding wild-type SHIP2 (WT-SHIP2) and a dominant-negative SHIP2 (ΔIP-SHIP2) were injected via the tail vein into db/+m and *db/db* mice, respectively. Four days later, amounts of hepatic SHIP2 protein were increased by fivefold. Insulin-induced phosphorylation of Akt in liver was impaired in WT-SHIP2–expressing db/+m mice, whereas the reduced phosphorylation was restored in ΔIP-SHIP2–expressing *db/db* mice. The abundance of mRNA for glucose-6-phosphatase (G6Pase) and PEPCK was increased, that for glucokinase (GK) was unchanged, and that for sterol regulatory element–binding protein 1 (SREBP)-1 was decreased in hepatic WT-SHIP2–overexpressing db/+m mice. The increased expression of mRNA for G6Pase and PEPCK was partly suppressed, that for GK was further enhanced, and that for SREBP1 was unaltered by the expression of ΔIP-SHIP2 in *db/db* mice. The hepatic expression did not affect insulin signaling in skeletal muscle and fat tissue in both mice. After oral glucose intake, blood glucose levels and plasma insulin concentrations were elevated in WT-SHIP2–expressing db/+m mice, while elevated values were decreased by the expression of ΔIP-SHIP2 in *db/db* mice. These results indicate that hepatic SHIP2 has an impact in vivo on the glucose metabolism in both physiological and diabetic states possibly by regulating hepatic gene expression. *Diabetes* 54:1958–1967, 2005

From the [1]First Department of Internal Medicine, Toyama Medical & Pharmaceutical University, Toyama, Japan; the [2]Department of Clinical Pharmacology, Toyama Medical & Pharmaceutical University, Toyama, Japan; and [3]Sainou Hospital, Toyama, Japan.

Address correspondence and reprint requests to Toshiyasu Sasaoka, MD, PhD, Department of Clinical Pharmacology, Toyama Medical & Pharmaceutical University, 2630 Sugitani, Toyama, 930-0194, Japan. E-mail: tsasaoka-tym@umin.ac.jp.

Received for publication 15 November 2004 and accepted in revised form 11 April 2005.

G6Pase, glucose-6-phosphatase; GK, glucokinase; ΔIP-SHIP2, dominant-negative SHIP2; IRS, insulin receptor substrate; PI, phosphatidylinositol; PTEN, 3′-lipid phosphatase; SHIP2, SH2-containing inositol 5′-phosphatase 2; SREBP, sterol regulatory element–binding protein; WT-SHIP2, wild-type SHIP2.

Insulin binding to the insulin receptor in turn phosphorylates insulin receptor substrates (IRSs) at tyrosine residues (1,2). The tyrosine-phosphorylated IRS binds to the p85 regulatory subunit of phosphatidylinositol (PI) 3-kinase, resulting in the activation of the p110 subunit (3,4). PI 3-kinase functions as a lipid kinase to produce $PI(3,4,5)P_3$ from $PI(4,5)P_2$ in vivo (5). $PI(3,4,5)P_3$ is crucial as a lipid second messenger in various metabolic effects of insulin (3,6–8). $PI(3,4,5)P_3$ mediates insulin signals to downstream molecules including Akt (9). Akt is the key signaling molecule in the activation of glucose uptake in the skeletal muscle and fat tissue and in the regulation of mRNA expression for gluconeogenesis, glycolysis, and lipid synthesis in the liver (10). SH2-containing inositol 5′-phosphatase 2 (SHIP2) was identified as a lipid phosphatase that hydrolyzes $PI(3,4,5)P_3$ to $PI(3,4)P_2$ (11,12). Targeted disruption of the SHIP2 gene in mice caused an increase in insulin sensitivity without affecting other biological systems (13). In addition, some polymorphisms of the SHIP2 gene found in British and French populations are associated with metabolic syndromes including type 2 diabetes and hypertension (14). The expression of SHIP2 could be elevated in type 2 diabetic subjects with a 16-bp deletion in the 3′-untranslated regulatory region of the SHIP2 gene (15). Based on these reports, SHIP2 appears to be a physiologically important negative regulator relatively specific to insulin signaling with an impact on the state of insulin resistance (13–17).

We have previously reported that overexpression of SHIP2, via 5′-phosphatase activity, impaired insulin-induced activation of Akt resulting in decreased glucose uptake and glycogen synthesis in 3T3-L1 adipocytes and L6 myocytes (18,19). Although we clarified the role and molecular mechanisms by which SHIP2 regulates insulin signaling in the skeletal muscle and fat tissue (20–22), the impact of SHIP2 in the liver on the metabolism of glucose in vivo is largely unknown. Based on studies with tissue-specific knockout of the insulin receptor in mice, the liver was found to be the most critical target tissue of insulin action in the control of glucose homeostasis (23,24). Insulin regulates hepatic glucose output through suppression of hepatic gluconeogenic gene expression via the IRS-2/PI 3-kinase pathway and augmentation of glycolytic gene expression via the IRS-1/PI 3-kinase pathway (25–30).

Sterol regulatory element–binding protein (SREBP)-1c is the key factor involved in insulin resistance by controlling lipid synthesis via the IRS-1/PI 3-kinase pathway (30). On the basis of these results, it is possible that SHIP2 in the liver functions as a negative regulator of the PI 3-kinase–dependent metabolic action of insulin. Therefore, it would be of particular importance to clarify the impact of hepatic SHIP2 on the regulation of insulin signaling and hepatic gene expression for the control of glucose homeostasis in diabetic model mice as well as in nondiabetic mice.

In the present study, we investigated the impact of liver-specific overexpression of SHIP2 in lean db/+m mice and liver-specific inhibition of SHIP2 in diabetic *db/db* mice. Adenoviral vectors encoding wild-type SHIP2 (WT-SHIP2) and the dominant-negative mutant of SHIP2 (ΔIP-SHIP2) were injected, via the tail vein, into the db/+m and *db/db* mice, respectively. We studied the effect of hepatic SHIP2 expression on insulin signaling leading to hepatic gene expression. In addition, we examined whether the liver-specific expression of SHIP2 affects the metabolic actions of insulin in skeletal muscle and fat tissue. Furthermore, glucose metabolism was investigated by conducting glucose tolerance tests and insulin tolerance tests in WT-SHIP2–expressing db/+m and ΔIP-SHIP2–expressing *db/db* mice.

RESEARCH DESIGN AND METHODS

Human regular insulin HumalinR was provided by Eli Lilly. A polyclonal anti–IRS-1 antibody and a polyclonal anti-Thr^{308} phospho-specific Akt antibody were purchased from Cell Signaling Technology (Beverly, MA). A polyclonal anti–IRS-2 antibody and a polyclonal anti-Ser^{473} phospho-specific Akt antibody were obtained from Upstate Biotechnology (Lake Placid, NY). A polyclonal anti-Akt antibody was purchased from Santa Cruz Biotechnology (Santa Cruz, CA). A monoclonal anti-phosphotyrosine antibody (PY99) was purchased from Transduction Laboratories (Lexington, KY). The polyclonal anti-SHIP2 antibody has been described previously (12). Enhanced chemiluminescence reagents were obtained from Amersham Pharmacia Biotech (Uppsala, Sweden). All other routine reagents were of analytical grade and purchased from Sigma Chemicals (St. Louis, MO) or Wako Pure Chemical Industries (Osaka, Japan).

Male C57BL/KsJ-*db/db* Jcl (BKS.Cg-+*Lep^{db}*/+*Lepr^{db}*/Jcl) mice, their lean heterozygote littermates (*db/+m*), and C57BL/6J mice were purchased from Clea Japan (Tokyo, Japan) at 6 weeks of age. Mice were maintained under standard light (12 h light/dark) and temperature conditions. These mice were caged in groups of four and were provided with standard rodent diet and water ad libitum.

Adenovirus-mediated gene transfer in the liver. Adenoviral vectors encoding rat WT-SHIP2 and a PI 5′-phosphatase–defective ΔIP-SHIP2 have been described previously (18). Eight-week-old male mice were injected with the adenovirus via the tail vein at a concentration of 5×10^8 pfu (plaque-forming units)/g body wt in a suspension of 200 μl PBS. Experiments were performed 4 days after the injection. All procedures were approved by the Committee of Animal Experiments at Toyama Medical & Pharmaceutical University.

Western blot analysis. Mice deprived of food for 16 h were injected with human regular insulin (5 units/kg body wt) or saline via the tail vein. After 5 min, the mice were anesthetized and killed to isolate the liver, hindlimb muscle, and epididymal fat. These tissues were homogenized using a polytron at half-maximal speed (15,000 rpm) for 1 min on ice in 500 μl of a homogenization buffer containing 20 mmol/l Tris, 5 mmol/l EDTA, 10 mmol/l $Na_4P_2O_7$, 100 mmol/l NaF, 2 mmol/l Na_3VO_4, 1% NP-40, 1 mmol/l phenylmethylsulfonyl fluoride, 10 μg/ml aprotinin, and 10 μg/ml leupeptin (pH 7.5). The tissue lysates were solubilized by continuous stirring for 1 h at 4°C and centrifuged for 30 min at 14,000*g*. The supernatants (200 μg protein) were immunoprecipitated with indicated antibodies for 2 h at 4°C. The precipitates or the lysates were separated by 7.5% SDS-PAGE and transferred onto polyvinylidene difluoride membranes using a Bio-Rad Transblot apparatus. The membranes were blocked in a buffer containing 50 mmol/l Tris, 150 mmol/l NaCl, 0.1% Tween 20, and 5% nonfat milk (pH 7.5) for 2 h at 20°C. They were then probed with antibodies for 16 h at 4°C. After the membranes had been washed in a buffer containing 50 mmol/l Tris, 150 mmol/l NaCl, and 0.1% Tween 20 (pH 7.5), blots were incubated with horseradish peroxidase–linked second antibody and then examined by enhanced chemiluminescence (ECL) detection using an ECL reagent according to the manufacturer's instructions (Amersham). In each experiment, the intensity of the band derived from insulin-induced phosphorylation of IRS-1, IRS-2, and Akt in control db/+m mice was assigned as a value of 1 arbitrary unit, and the intensity of all treated groups in *db/db* mice was expressed as a fold value of control.

Northern blot analysis. Mice deprived of food for 16 h were anesthetized and killed, and the liver was removed and frozen in liquid N2. Mice were not fasted for the analysis of SREBP1 mRNA. Total RNA was extracted from 50 mg of the liver sample using the QuickPrep total RNA Extraction Kit (Amersham). Total RNA (10 μg) for each sample was separated using a 1% agarose gel and transferred to a Hybond-H$^+$ positively charged nylon membrane (Amersham). Probes for glucokinase (GK) (31), SREBP-1 (32), PEPCK (33), glucose-6-phosphatase (G6Pase) (34), and Glut2 (35) mRNAs were kindly provided by T. Noguchi (Nagoya University, Nagoya, Japan), H. Shimano (Tsukuba University, Ibaragi, Japan), D.K. Granner (Vanderbilt University Medical Center, Nashville, TN), H. Nakajima (Osaka Medical Center for Cancer and Cardiovascular Disease, Osaka, Japan), and W. Ogawa (Kobe University, Kobe, Japan), respectively. Each probe was chemiluminescently labeled and hybridized, and the mRNA expression was detected using the AlkPhos Direct Labeling and Detection System with CDP-Star (Amersham Biosciences).

Oral glucose tolerance test and insulin tolerance test. For the oral glucose tolerance test, mice deprived of food for 16 h were loaded orally with glucose (2 g/kg). Blood samples were collected from the orbital sinus at various time points after the loading. For the insulin tolerance test, mice deprived of food for 8 h were injected intraperitoneally with human regular insulin (0.75 units/kg). Blood samples were collected from the tail vein at various time points. Blood glucose levels were then measured with a FreeStyle KISSEI (Kissei, Japan), and blood insulin concentrations were measured with an enzyme-linked immunosorbent assay kit (Morinaga, Japan).

Statistical analysis. Data are presented as means ± SE. P values were determined using a paired t test or Bonferroni test with ANOVA. $P < 0.05$ was considered statistically significant.

RESULTS

Expression of SHIP2 in the liver of mice injected with an adenoviral vector via the tail vein. Systemic adenoviral injection into mice via the tail vein is known to result in the liver-specific expression of the exogenous gene (36). The 5′-phosphatase–defective ΔIP-SHIP2 acts as a dominant-negative mutant possibly by competing with endogenous SHIP2 to bind PI(3,4,5)P_3 (18). By inhibiting the endogenous function of SHIP2, ΔIP-SHIP2 augments insulin signaling mediated by the PI 3-kinase product PI(3,4,5)P_3 (18,19). Hepatic expression of both WT-SHIP2 and ΔIP-SHIP2 was detected 1 day after the adenoviral injection. The abundance was maximal at 4 days, decreased thereafter, and returned to the basal level at 14 days after the injection (data not shown). Therefore, we examined the expression of WT-SHIP2 and ΔIP-SHIP2 in various tissues of mice 4 days after the adenoviral injection. As shown in Fig. 1, we observed fivefold greater amounts of exogenous WT-SHIP2 and ΔIP-SHIP2 than endogenous SHIP2 in the liver. The lower band seen in the liver of mice may be a splicing variant of SHIP2. Alternatively, we cannot rule out the possibility that the band originated from the degradation of SHIP2 during the preparation of samples. Except for the liver, expression of either exogenous WT-SHIP2 or ΔIP-SHIP2 was not detectable in the various tissues examined. The body weight of the mice was not changed by the liver-specific expression of SHIP2 (data not shown). We analyzed the effect of liver-specific expression of WT-SHIP2 in control db/+m mice and ΔIP-SHIP2 in diabetic *db/db* mice on the metabolic action of insulin.

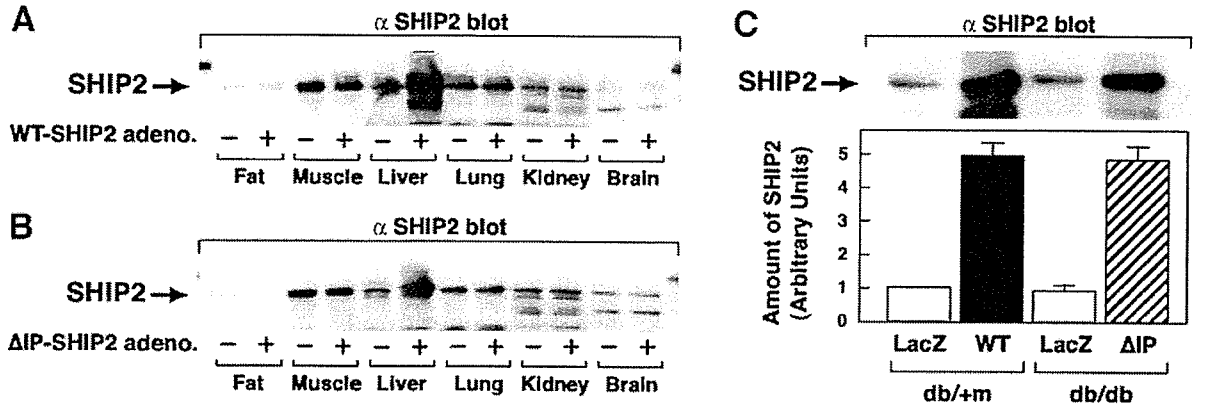

FIG. 1. Expression of SHIP2 in the liver of mice injected with an adenoviral vector via the tail vein. Total homogenates of the indicated tissues obtained from db/+m and *db/db* mice 4 days after adenoviral injection with WT-SHIP2 (*A*) and ΔIP-SHIP2 (*B*), respectively, were subjected to immunoblot analysis with anti-SHIP2 antibody. The amount of SHIP2 in the liver is shown as means ± SE of three separate experiments (*C*).

Effect of WT-SHIP2 expression on insulin-induced phosphorylation of IRS and Akt in the liver of db/+m mice. Mice injected with the adenoviral vector encoding WT-SHIP2 or control LacZ were deprived of food for 16 h and then injected intravenously with insulin (5 units/kg) or saline (200 μl) for 5 min. Thereafter, the liver was removed and subjected to immunoblot analysis (Fig. 2). Amounts of IRS-1, IRS-2, and Akt were not altered by expression of WT-SHIP2 in the liver of db/+m mice (Fig. 2*A–C*). Insulin-induced tyrosine phosphorylation of IRS-1 and IRS-2 was also comparable between WT-SHIP2– and LacZ-injected db/+m mice (Figs. 2*A* and *B*). Akt is a crucial mediator of IRS/PI 3-kinase signaling and is known to be activated by phosphorylation at Thr^{308} and Ser^{473} residues (10,37,38). Insulin induced phosphorylation of Akt at Thr^{308} in the liver of LacZ-transfected db/+m mice. The extent of the phosphorylation was decreased by 49.0 ± 13.0% in the liver of WT-SHIP2–overexpressing db/+m mice (Fig. 2*C*). Similar results were obtained in C57BL/6J mice (data not shown).

Effect of ΔIP-SHIP2 expression on insulin-induced phosphorylation of IRS and Akt in the liver of *db/db* mice. We next examined the ameliorative effect of the liver-specific expression of ΔIP-SHIP2 on the metabolic signaling of insulin in the liver of diabetic *db/db* mice (Fig. 3). In *db/db* mice, the amount of IRS-1 and IRS-2 was decreased by 27.9 ± 4.8 and 73.6 ± 5.2%, respectively, compared with db/+m mice, whereas the amount of Akt

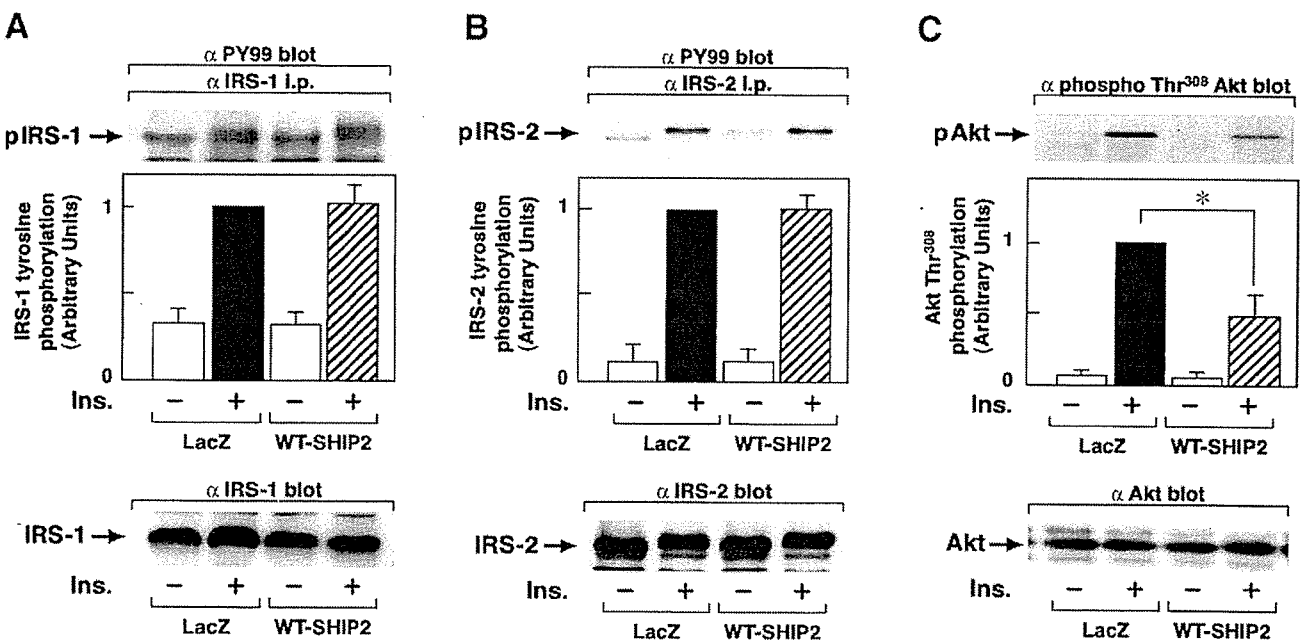

FIG. 2. Effect of WT-SHIP2 expression on insulin (Ins.)-induced phosphorylation of IRS and Akt in the liver of db/+m mice. WT-SHIP2– and LacZ-injected db/+m mice starved for 16 h were injected with insulin (5 units/kg) via the tail vein. After 5 min, the liver was excised and homogenized. Tissue samples were immunoprecipitated with anti–IRS-1 antibody (*A*) or anti–IRS-2 antibody (*B*). The precipitates were subjected to immunoblot analysis with the same antibodies or anti-phosphotyrosine antibody. The tissue samples were subjected to immunoblot analysis with anti-Akt antibody or anti–phospho-Thr^{308}–specific Akt antibody (*C*). Results are means ± SE of four separate experiments. **P* < 0.05 vs. the amount of Akt phosphorylated in LacZ-transfected mice. i.p., intraperitoneal.

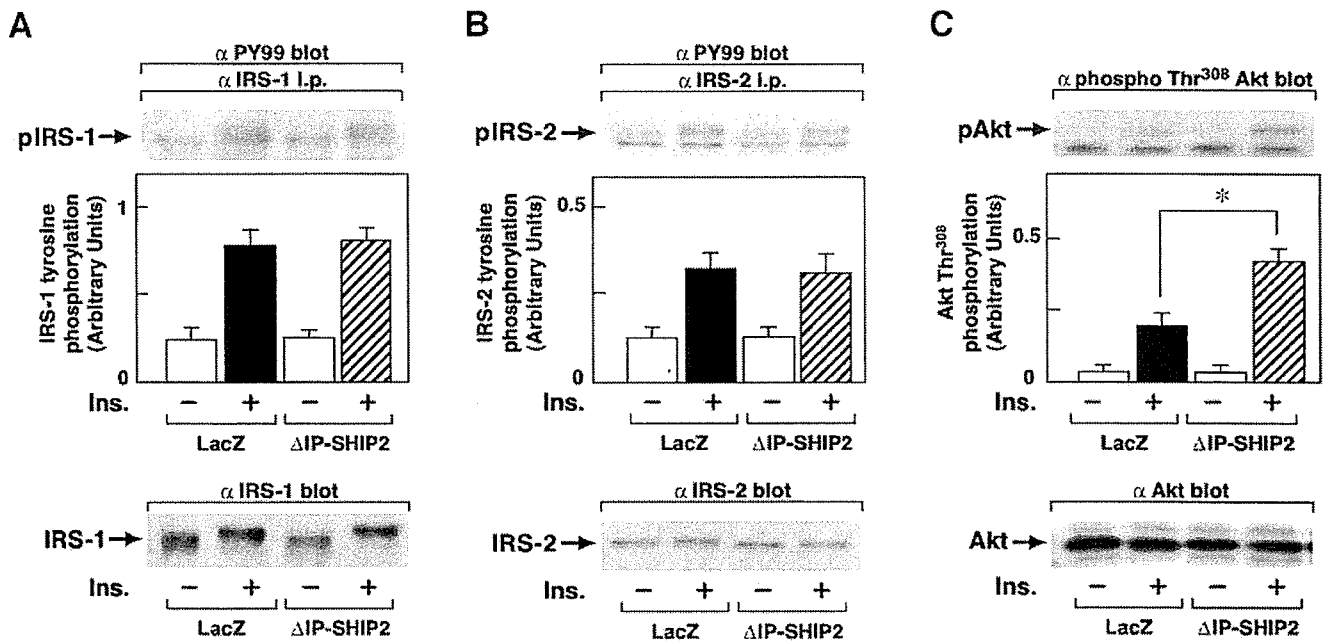

FIG. 3. Effect of ΔIP-SHIP2 expression on insulin (Ins.)-induced phosphorylation of IRS and Akt in the liver of diabetic *db/db* mice. ΔIP-SHIP2– and LacZ-injected *db/db* mice starved for 16 h were injected with insulin (5 units/kg) via the tail vein. After 5 min, the liver was excised and homogenized. Tissue samples were immunoprecipitated with anti–IRS-1 antibody (*A*) or anti–IRS-2 antibody (*B*). The precipitates were subjected to immunoblot analysis with the same antibodies or anti-phosphotyrosine antibody. The tissue samples were subjected to immunoblot analysis with anti-Akt antibody or anti–phospho-Thr^{308}–specific Akt antibody (*C*). Results are means ± SE of four separate experiments. *$P < 0.05$ vs. the amount of Akt phosphorylated in LacZ-transfected mice. i.p., intraperitoneal.

was not altered (data not shown). Consistent with the results in Fig. 2, amounts of IRS-1, IRS-2, and Akt in the liver were not changed by the expression of ΔIP-SHIP2 in *db/db* mice compared with that in LacZ-injected *db/db* mice (Fig. 3*A–C*). Insulin-induced phosphorylation of Akt at Thr^{308} was decreased in *db/db* mice to 19.7 ± 5.0% of that in control db/+m mice. Interestingly, the extent of phosphorylation was restored to 45.2 ± 4.5% by expression of ΔIP-SHIP2 in the liver of *db/db* mice (Fig. 3*C*). In addition, the degree of change in the phosphorylation of Akt well paralleled the alteration of Akt activity in both db/+m and *db/db* mice (data not shown). Furthermore, similar results were seen in 5-h–fasted mice in addition to 16-h–fasted mice (data not shown). These results indicate that SHIP2 is involved in the regulation of insulin-induced phosphorylation of Akt in the liver of both nondiabetic and diabetic mice.

Effect of SHIP2 expression on the hepatic gene expression in db/+m mice and *db/db* mice. Because the metabolic effect of insulin in the liver is mainly regulated by the hepatic expression of genes involved in gluconeogenesis, glycolysis, and fat synthesis (29), we examined the effect of liver-specific SHIP2 expression on the insulin-induced regulation of the hepatic gene expression (Fig. 4*A–D*). We performed Northern blot analysis of total RNA isolated from the liver of db/+m mice and *db/db* mice. The level of G6Pase mRNA and PEPCK mRNA in the liver was increased by 179 ± 78 and 190 ± 57%, respectively, by the liver-specific expression of WT-SHIP2 in db/+m mice. On the other hand, the abundance of GK mRNA was not altered, and that of SREBP1 mRNA was decreased by 45.0 ± 6.5% by the expression. The levels of G6Pase, PEPCK, GK, and SREBP1 mRNAs in the liver were increased by 872 ± 59, 460 ± 49, 306 ± 26, and 120 ± 16%, respectively, in LacZ-transfected *db/db* mice compared with control db/+m mice. The enhanced expression of G6Pase mRNA and PEPCK mRNA was partly reduced by 23.0 ± 8.0 and 36.0 ± 13.0%, respectively, by the liver-specific expression of ΔIP-SHIP2 in *db/db* mice compared with that of LacZ-injected *db/db* mice. Conversely, the extent of GK mRNA expression in the liver was further enhanced by 31.0 ± 9.0% in the ΔIP-SHIP2–expressing *db/db* mice. Elevated expression of SREBP1 mRNA was not changed by the expression. On the other hand, although the expression of Glut2 mRNA in the liver was increased in *db/db* mice compared with db/+m mice, neither WT-SHIP2 nor ΔIP-SHIP2 expression affected the level of Glut2 mRNA (Fig. 4*E*). In addition, the abundance of r18S RNA was equal among the samples to ensure that the same amount of total RNA was used (Fig. 4*F*).

Liver-specific expression of SHIP2 did not affect insulin-induced phosphorylation of IRS and Akt in the skeletal muscle and fat tissue of db/+m and *db/db* mice. We further investigated whether the liver-specific expression of SHIP2 affects insulin signaling in skeletal muscle and fat tissue. The level of IRS-1 or Akt did not differ in the skeletal muscle of WT-SHIP2– and LacZ-expressing db/+m mice, and that of ΔIP-SHIP2– and LacZ-expressing *db/db* mice. In addition, no apparent difference was found in the amount of basal and insulin-induced phosphorylation of IRS-1 and Akt in the skeletal muscle of WT-SHIP2– and LacZ-expressing db/+m mice and in that of ΔIP-SHIP2– and LacZ-expressing *db/db* mice (Fig. 5). Similarly, neither the amount nor the extent of insulin-induced phosphorylation of IRS-1 and Akt differed in the fat tissue of WT-SHIP2– and LacZ-expressing db/+m

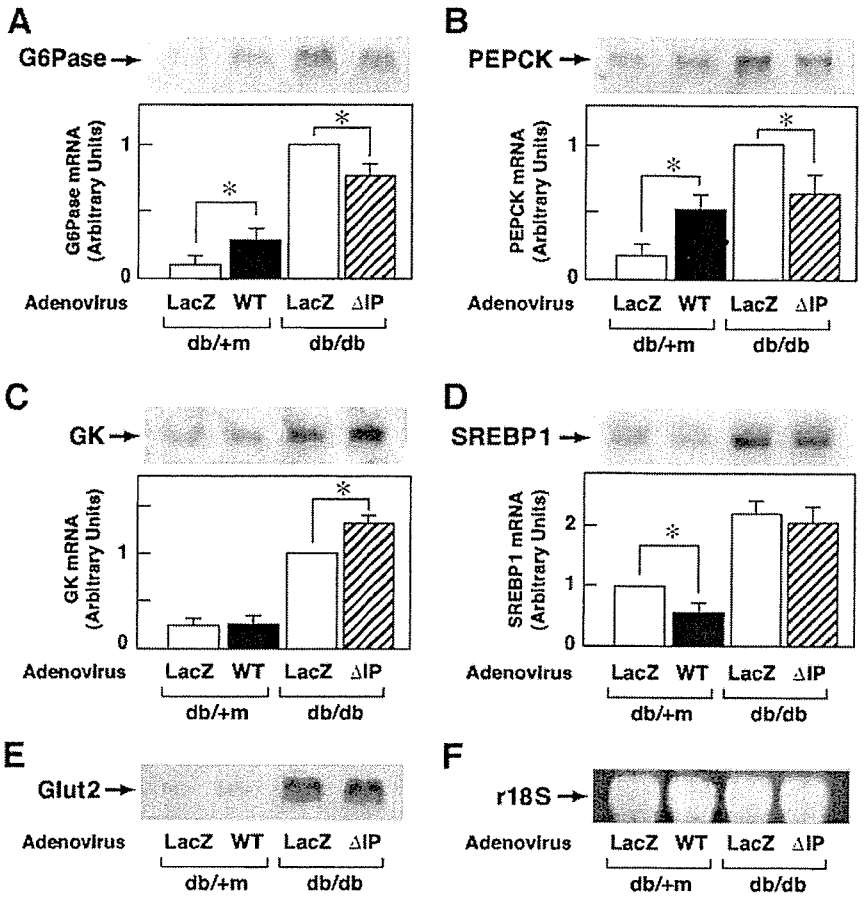

FIG. 4. Effect of SHIP2 expression on hepatic gene expression in db/+m mice and *db/db* mice. Total RNA isolated from the liver of WT-SHIP2– or LacZ-injected db/+m mice and ΔIP-SHIP2– or LacZ-injected *db/db* mice was subjected to Northern blotting with probes for G6Pase (*A*), PEPCK (*B*), GK (*C*), SREBP1 (*D*), and Glut2 (*E*) mRNAs and r18S (*F*). Results are representative of four separate experiments and shown as means ± SE **P* < 0.05 vs. the level of expression in LacZ-transfected mice.

mice and in that of ΔIP-SHIP2– and LacZ-expressing *db/db* mice (Fig. 6).

Blood glucose and plasma insulin concentrations during oral glucose tolerance and insulin tolerance tests in SHIP2-expressing db/+m and *db/db* mice. Because the liver-specific expression of SHIP2 affected hepatic insulin signaling leading to the altered expression of genes implicated in glucose homeostasis, we examined the effect of liver-specific SHIP2 expression on glucose and insulin tolerance in db/+m and *db/db* mice. The blood glucose concentration at 30 min after oral glucose intake was higher in WT-SHIP2–expressing db/+m mice than LacZ-expressing db/+m mice (Fig. 7*A*). Plasma insulin concentrations remained higher at 0, 15, and 30 min after the glucose loading in WT-SHIP2–expressing db/+m mice than in LacZ-expressing db/+m mice (Fig. 7*B*). The kinetics of blood glucose concentrations after the insulin injection was comparable between WT-SHIP2– and LacZ-expressing db/+m mice (Fig. 8*A*). On the other hand, the basal glucose concentration was significantly reduced and the plasma insulin concentration tended to be decreased in ΔIP-SHIP2–expressing *db/db* mice compared with LacZ-expressing *db/db* mice. In addition, blood glucose levels (Fig. 7*C*) and plasma insulin concentrations (Fig. 7*D*) were significantly lower in ΔIP-SHIP2–expressing *db/db* mice than in LacZ-injected *db/db* mice at 15, 30, and 60 min after oral glucose intake. Furthermore, blood glucose levels were lower in ΔIP-SHIP2–expressing *db/db* mice than in LacZ-expressing *db/db* mice before and after the insulin injection (Fig. 8*B*).

DISCUSSION

A previous study (13) with knockout mice demonstrated that SHIP2 plays an important role in the negative regulation of the metabolic action of insulin in vivo. SHIP2 also appears to be implicated in type 2 diabetes with insulin resistance (14,15). Although the functional impact of SHIP2 on insulin signaling has been studied in cultured fat and skeletal muscle cells in vitro (16–22), the impact in vivo of hepatic SHIP2 on glucose metabolism in nondiabetic and diabetic states is unknown. Thus, it would be interesting to clarify how a hepatic excess of SHIP2 promotes insulin resistance and how the inhibition of hepatic SHIP2 ameliorates glucose metabolism in a state of insulin resistance in mice. We have shown that the systemic infusion of adenoviral vectors encoding WT-SHIP2 and a dominant-negative mutant of SHIP2 (ΔIP-SHIP2) in mice resulted in liver-specific expression of the protein.

We utilized db/+m mice as an animal of lean nondiabetic control. The liver-specific overexpression of WT-SHIP2 impaired insulin-induced phosphorylation of Akt without affecting tyrosine phosphorylation of IRS-1 and IRS-2 in the liver. Approximately a 50% decrease in the phosphorylation of Akt was observed even after the overexpression of WT-SHIP2 to a level more than fivefold that of endogenous SHIP2, as shown in Fig. 2*C*. As a cause of partial inhibition of the phosphorylation, we assume that SHIP2 product PI(3,4)P2 has some signaling ability to transmit the signal for the phosphorylation of Akt, al-

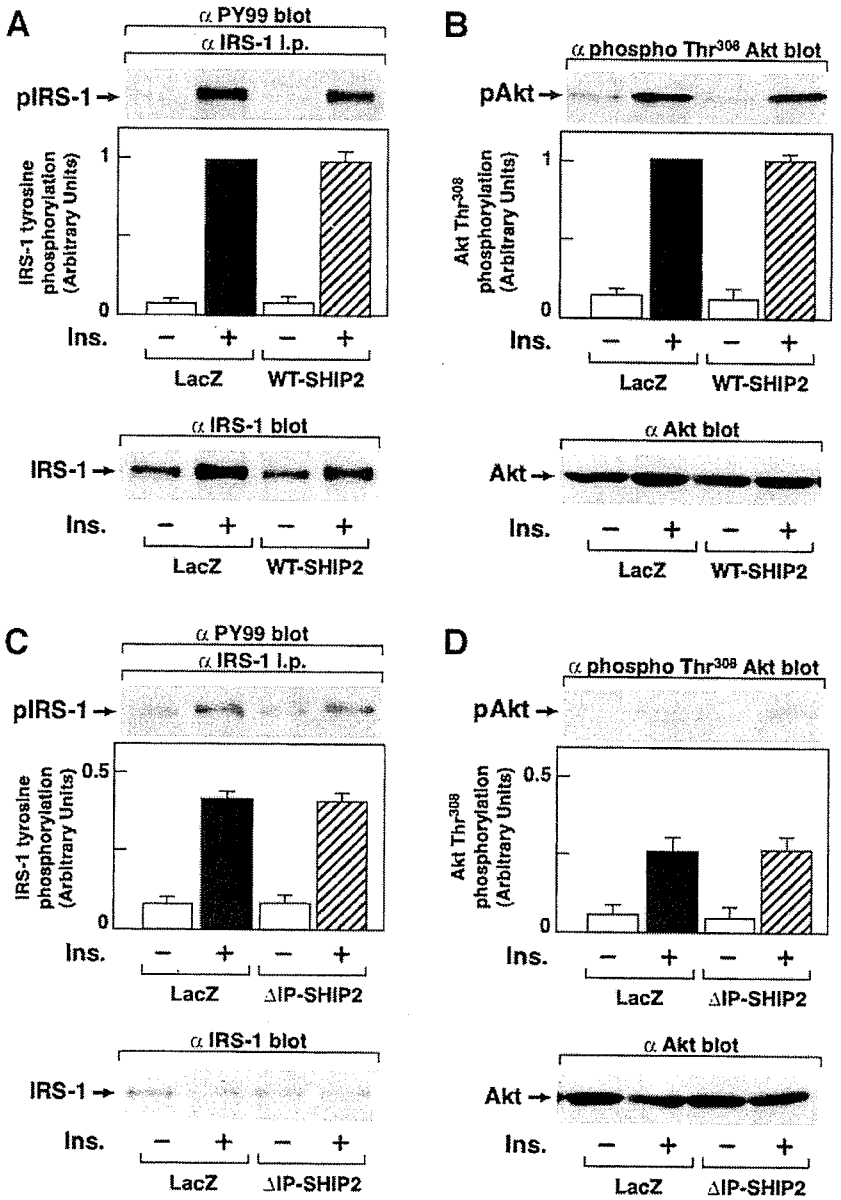

FIG. 5. Expression of SHIP2 did not alter insulin (Ins.)-induced phosphorylation of IRS and Akt in the skeletal muscle of db/+m and *db/db* mice. WT-SHIP2– or LacZ-injected db/+m mice (*A* and *B*), and ΔIP-SHIP2– or LacZ-injected *db/db* mice (*C* and *D*) starved for 16 h were injected with insulin (5 units/kg) via the tail vein. After 5 min, the skeletal muscle of the mice was excised and homogenized. Tissue samples were immunoprecipitated with anti–IRS-1 antibody. The precipitates were subjected to immunoblot analysis with anti–IRS-1 antibody or anti-phosphotyrosine antibody (*A* and *C*). The tissue samples were immunoblotted with anti-Akt antibody or anti–phospho-Thr^{308}–specific Akt antibody (*B* and *D*). Results are means ± SE of four separate experiments. *$P < 0.05$ vs. the amount of Akt phosphorylated in LacZ-transfected mice. i.p., intraperitoneal.

though less ability than PI(3,4,5)P3 (18,19). The overexpression of SHIP2 also resulted in hyperinsulinemia and potentiated the increase in blood glucose levels after oral glucose intake. These results indicate that the excess of SHIP2 in the liver can cause systemic insulin resistance through inhibition of hepatic Akt activation in vivo. Our results are consistent with a previous study (35) showing the effect of the liver-specific expression of a dominant-negative mutant of PI 3-kinase (Δp85), indicating that the hepatic PI 3-kinase pathway plays an essential role in the metabolic action of insulin. Thus, either inactivation of PI 3-kinase or potentiated hydrolysis of the PI 3-kinase product in the liver appears to result in an exacerbation of glucose metabolism in vivo.

We next studied *db/db* mice as an animal model of type 2 diabetes with insulin resistance. Db/db mice are obese and show hyperglycemia and hyperinsulinemia (39,40). The amount of protein and the extent of insulin-induced phosphorylation of IRS-1 and IRS-2 were mildly and markedly reduced, respectively, in the liver of *db/db* mice compared with that of db/+m mice. In addition, insulin-induced phosphorylation of Akt was markedly suppressed in the liver of *db/db* mice. Interestingly, the liver-specific expression of ΔIP-SHIP2 effectively restored the decreased phosphorylation of Akt without affecting the tyrosine phosphorylation of IRS-1 and IRS-2 in the liver. The hepatic expression of ΔIP-SHIP2 reduced fasting blood glucose concentrations and improved elevated glucose levels and insulin concentrations after oral glucose intake in *db/db* mice. Consistent with a recently published article (41) showing that an absence of SHIP2 confers resistance to diet-induced obesity and hyperglycemia in mice, our results indicate that the inhibition of endogenous SHIP2 in the liver can effectively ameliorate hyperglycemia and hyperinsulinemia through an improvement of the Akt pathway in diabetic *db/db* mice. In addition, these results

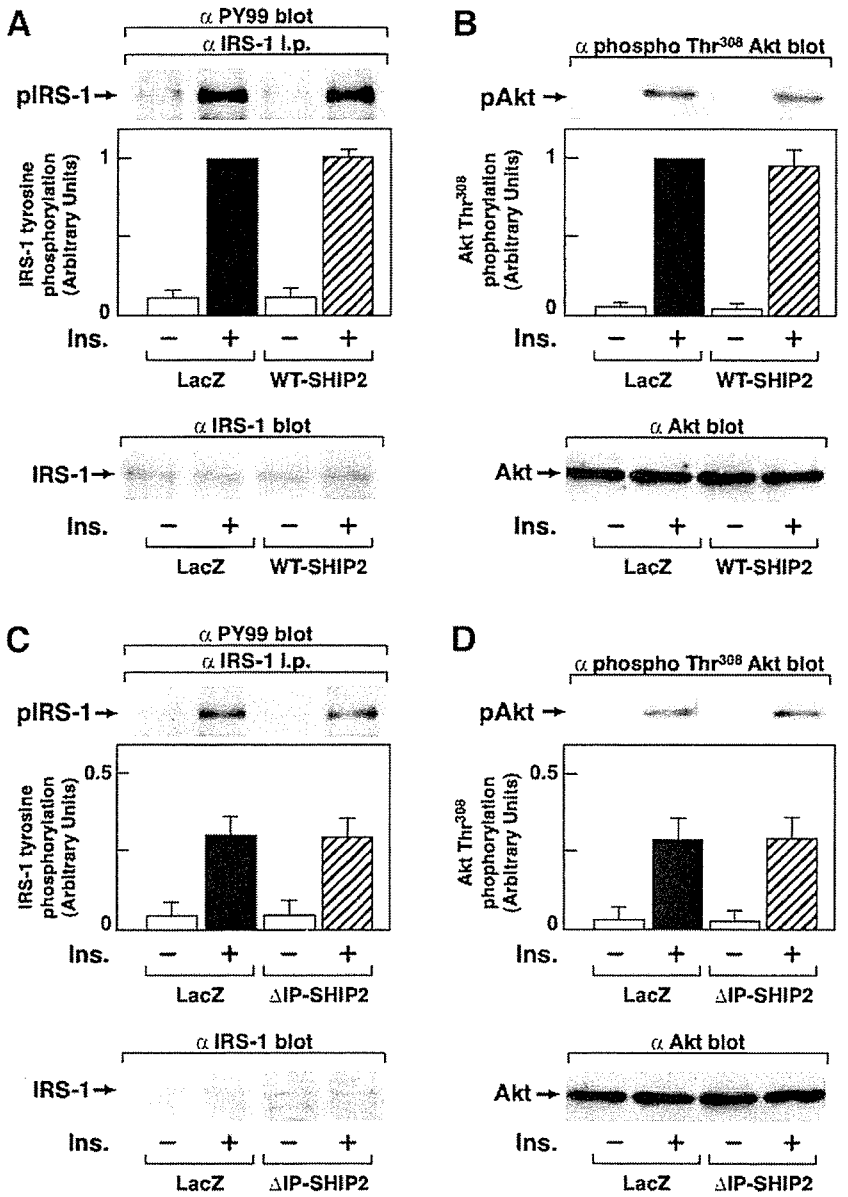

FIG. 6. Expression of SHIP2 did not alter insulin (Ins.)-induced phosphorylation of IRS and Akt in the fat tissue of db/+m and *db/db* mice. WT-SHIP2– or LacZ-injected db/+m mice (*A* and *B*), and ΔIP-SHIP2– or LacZ-injected *db/db* mice (*C* and *D*) starved for 16 h were injected with insulin (5 units/kg) via the tail vein. After 5 min, the epididymal fat of the mice was excised and homogenized. Tissue samples were immunoprecipitated with anti–IRS-1 antibody. The precipitates were subjected to immunoblot analysis with anti–IRS-1 antibody or anti-phosphotyrosine antibody (*A* and *C*). The tissue samples were immunoblotted with anti-Akt antibody or anti–phospho-Thr^{308}-specific Akt antibody (*B* and *D*). Results are means ± SE of four separate experiments. **P* < 0.05 versus the amount of Akt phosphorylated in LacZ-transfected mice.

are consistent with reports on the 3′-lipid phosphatase PTEN. The PI 3-kinase product PI(3,4,5)P3 can also be hydrolyzed by PTEN (42). Thus, inhibition of PTEN was found to enhance insulin signaling in the liver in studies using tissue-specific deletion and antisense approaches (43,44).

Tissue-specific knockout of the insulin receptor revealed the liver to be the most crucial organ in terms of glucose metabolism in vivo (23,24). Insulin regulates glucose metabolism in the liver by regulating hepatic gene expression (23,24). The conversion of glucose to glucose 6-phosphate catalyzed by GK is the initial step in the utilization of glucose (45). Conversely, the reaction catalyzed by G6Pase is the final step of in the production of glucose, and PEPCK is a rate-controlling enzyme of gluconeogenesis in the liver (29). In addition, the production of triglycerides is mediated by lipogenic enzymes mainly regulated in a SREBP1c-dependent manner in the liver, and the enhanced expression of SREBP1c is associated with insulin resistance by causing fatty liver (46). Insulin is known to rapidly inhibit hepatic gluconeogenic gene expression and suppress hepatic glucose output via an IRS-2–mediated PI 3-kinase–dependent pathway mainly involved in Akt signaling (25–28). On the other hand, insulin increases the expression of GK mRNA and SREBP1c mRNA via the IRS-1–PI 3-kinase pathway (30). Based on these findings, inappropriate increases in the mRNA expression of G6Pase, PEPCK, and SREBP1c and/or a reduction in the mRNA expression of GK can lead to systemic insulin resistance (29,45–48). Along these lines, transgenic mice with hepatic overexpression of G6Pase or PEPCK exhibited enhanced hepatic glucose output leading to hyperinsulinemia and hyperglycemia (49,50).

Our results show that the hepatic expression of G6Pase and PEPCK mRNAs was increased by the hepatic overex-

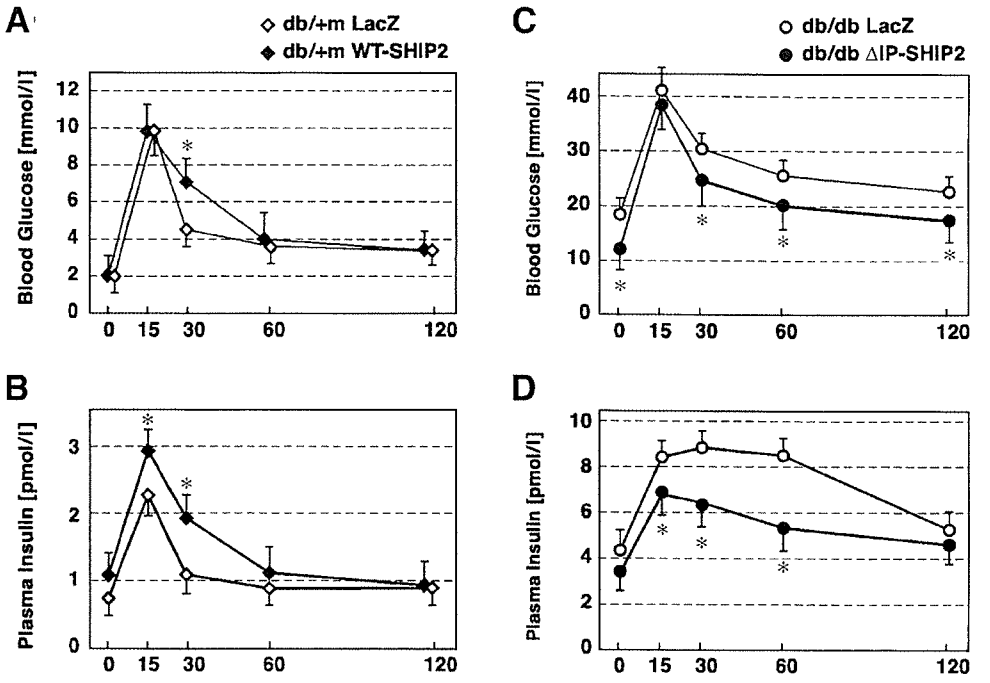

FIG. 7. Blood glucose and plasma insulin concentrations during oral glucose tolerance tests in SHIP2-expressed mice. WT-SHIP2– and LacZ-injected db/+m mice (*A* and *B*) and ΔIP-SHIP2– and LacZ-injected *db/db* mice (*C* and *D*) were starved for 16 h and then loaded orally with glucose (2 g/kg). Blood glucose levels (*A* and *C*) and plasma insulin concentrations (*B* and *D*) were measured at the indicated times after glucose loading. Results are means ± SE of four separate experiments. **P* < 0.05 vs. the corresponding value in LacZ-transfected mice.

pression of SHIP2 in db/+m mice. The apparent increase in blood glucose levels after the oral intake of glucose in the WT-SHIP2–expressing db/+m mice may be due to an impaired regulation of gluconeogenic gene expression leading to a reduced ability of the liver to dispose of glucose. The abundance of SREBP1 mRNA was reduced and that of GK mRNA was unaltered in the liver of WT-SHIP2–expressing db/+m mice. Based on the data, although the hepatic overexpression of WT-SHIP2 appears to regulate lipid synthesis through SREBP1c, the effect may have less of an impact on glucose metabolism than that caused by the altered levels of G6Pase and PEPCK mRNAs in the liver. On the other hand, the abundance of G6Pase, PEPCK, GK, and SREBP1c mRNAs was significantly increased in the liver of diabetic *db/db* mice. The inappropriately enhanced expression of G6Pase and PEPCK mRNAs was partially ameliorated, that of SREBP1 mRNA was unaltered, and that of GK mRNA was further increased in the liver of ΔIP-SHIP2–expressing *db/db* mice. Because these alterations of G6Pase, PEPCK, and GK mRNA expression are able to improve hepatic glucose disposal, the effect of hepatic ΔIP-SHIP2 expression on the improvement of hyperglycemia and hyperinsulinemia is considered to be mainly attributable to these changes in *db/db* mice. Notably, since hepatic glucose production is controlled by the expression of G6Pase and PEPCK in the liver, the improvement of glucose metabolism appears to be mainly caused by the inhibition of hepatic SHIP2 function leading to the appropriate regulation of hepatic glucose production. Fatty liver is possibly a result of the enhanced expression of SREBP1c mRNA in *db/db* mice. Since SREBP1 mRNA is already highly expressed in *db/db* mice, the enhanced PI 3-kinase–dependent signaling caused by the expression of ΔIP-SHIP2 may not have the effect of altering the expression of SREBP1 mRNA. Consistent with this interpretation, the extent of fatty liver was apparently unchanged by the expression of hepatic ΔIP-SHIP2 in *db/db* mice based on the histological analysis (data not shown).

After the oral intake of glucose, blood glucose levels and

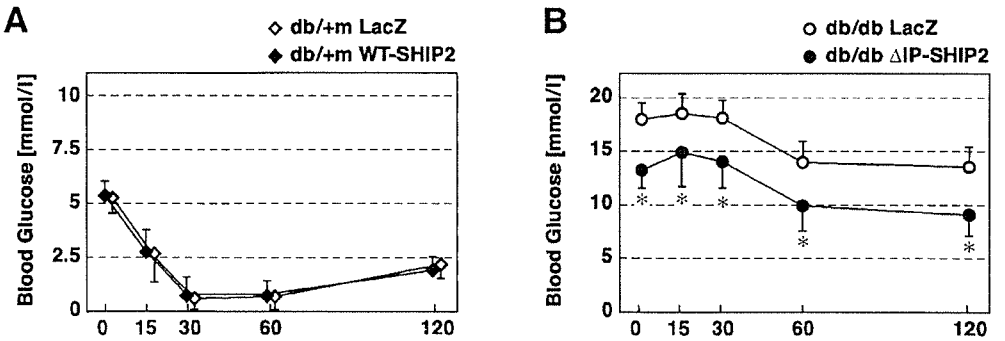

FIG. 8. Blood glucose levels during insulin tolerance tests in SHIP2-expressed mice. WT-SHIP2– and LacZ-injected db/+m mice (*A*) and ΔIP-SHIP2– and LacZ-injected *db/db* mice (*B*) were starved for 8 h and then injected intraperitoneally with insulin (0.75 units/kg). Blood glucose levels were measured at the indicated times after insulin injection. Results are means ± SE of four separate experiments. **P* < 0.05 vs. the corresponding value in LacZ-transfected mice.

serum insulin concentrations were elevated by the liver-specific expression of WT-SHIP2 in db/+m mice, but the increases were ameliorated by the liver-specific expression of ΔIP-SHIP2 in *db/db* mice. In contrast, blood glucose levels after intraperitoneal insulin injection were comparable between control LacZ- and WT-SHIP2–expressing db/+m mice. Fasting blood glucose levels were decreased by the hepatic expression of ΔIP-SHIP2 in *db/db* mice. The degree of the decrease in blood glucose levels appeared similar between LacZ- and ΔIP-SHIP2–expressing *db/db* mice at all time points after the intraperitoneal insulin injection. Because glucose levels after the intraperitoneal injection of insulin are mainly attributable to the effect of insulin on skeletal muscle and fat tissue (35), our results indicate that the effect of liver-specific expression of SHIP2 may be limited to the hepatic actions of insulin without affecting actions in the skeletal muscle and fat tissue. In this regard, insulin-induced tyrosine phosphorylation of IRS-1 and IRS-2 and phosphorylation of Akt at Thr^{308} and Ser^{473} were not affected in the skeletal muscle and fat tissue by the liver-specific expression of either WT-SHIP2 in db/+m mice or ΔIP-SHIP2 in *db/db* mice (Figs. 5 and 6 and data not shown). Our results partly contrast with a previous report (35) on the effect of liver-specific expression of Δp85. Inhibition of hepatic PI 3-kinase for 3 days affected insulin signaling in fat tissue, but not in skeletal muscle, to some extent (35). These possible differences may arise from the relatively minor alterations of blood glucose levels and insulin concentrations caused by the expression of WT-SHIP2 compared with those caused by the expression of Δp85. In this context, we cannot rule out the possibility that the skeletal muscle and/or fat tissue are involved, at least in part, in the alteration of glucose homeostasis caused by the liver-specific expression of SHIP2 in mice. More studies will be necessary to clarify this issue.

In summary, our results indicate that *1*) the liver-specific expression of SHIP2 regulates insulin-induced phosphorylation of Akt in the liver, but not in the skeletal muscle and fat tissue, *2*) elevation of SHIP2 expression in the liver has an impact on the deterioration of glucose metabolism in vivo, and *3*) the inhibition of SHIP2 function in the liver is an effective approach for the amelioration of hyperglycemia with insulin resistance.

ACKNOWLEDGMENTS

This work was supported in part by a Grant-in-Aid for Scientific Research from the Japan Society for the Promotion of Science and by a grant for research on sensory and communicative disorders by the Ministry of Health, Labor, and Welfare, Japan.

REFERENCES

1. Khan AH, Pessin JE: Insulin regulation of glucose uptake: a complex interplay of intracellular signalling pathways. *Diabetologia* 45:1475–1483, 2002
2. Saltiel AR, Kahn CR: Insulin signalling and the regulation of glucose and lipid metabolism. *Nature* 414:799–806, 2001
3. White MF: IRS proteins and the common path to diabetes. *Am J Physiol Endocrinol Metab* 283:E413–E422, 2002
4. Cantley LC: The phosphoinositide 3-kinase pathway. *Science* 296:1655–1657, 2002
5. Shepherd PR, Withers DJ, Siddle K: Phosphoinositide 3-kinase: the key switch mechanism in insulin signalling. *Biochem J* 333:471–490, 1998
6. Ueki K, Fruman DA, Brachmann SM, Tseng Y-H, Cantley LC, Kahn CR: Molecular balance between the regulatory and catalytic subunits of phosphoinositide 3-kinase regulates cell signaling and survival. *Mol Cell Biol* 22:965–977, 2002
7. Stokoe D, Stephens LR, Copeland T, Gaffney PRJ, Reese CB, Painter GF, Holmes AB, McCormick F, Hawkins PT: Dual role of phosphatidylinositol-3,4,5-trisphosphate in the activation of protein kinase B. *Science* 277:567–570, 1997
8. Sweeney G, Garg RR, Ceddia RB, Li D, Ishiki M, Somwar R, Foster LJ, Neilsen PO, Prestwich GD, Rudich A, Klip A: Intracellular delivery of phosphatidylinositol (3,4,5)-trisphosphate causes incorporation of glucose transporter 4 into the plasma membrane of muscle and fat cells without increasing glucose uptake. *J Biol Chem* 279:32233–32242, 2004
9. Milburn CC, Deak M, Kelly SM, Price NC, Alessi DR, Van Aalten DM: Binding of phosphatidylinositol 3,4,5-trisphosphate to the pleckstrin homology domain of protein kinase B induces a conformational change. *Biochem J* 375:531–538, 2003
10. Hanada M, Feng J, Hemmings BA: Structure, regulation and function of PKB/AKT: a major therapeutic target. *Biochim Biophys Acta* 1697:3–16, 2004
11. Pesesse X, Deleu S, De Smedt F, Drayer L, Erneux C: Identification of a second SH2-domain-containing protein closely related to the phosphatidylinositol polyphosphate 5-phosphatase SHIP. *Biochem Biophys Res Commun* 239:697–700, 1997
12. Ishihara H, Sasaoka T, Hori H, Wada T, Hirai H, Haruta T, Langlois WJ, Kobayashi M: Molecular cloning of rat SH2-containing inositol phosphatase 2 (SHIP2) and its role in the regulation of insulin signaling. *Biochem Biophys Res Commun* 260:265–272, 1999
13. Clément S, Krause U, Desmedt F, Tanti J-F, Behrends J, Pesesse X, Sasaki T, Penninger J, Doherty M, Malaisse W, Dumont JE, Le Marchand-Brustel Y, Erneux C, Hue L, Schurmans S: The lipid phosphatase SHIP2 controls insulin sensitivity. *Nature* 409:92–97, 2001
14. Kaisaki PJ, Delépine M, Woon PY, Sebag-Montefiore L, Wilder SP, Menzel S, Vionnet N, Marion E, Riveline J-P, Charpentier G, Schurmans S, Levy JC, Lathrop M, Farrall M, Gauguier D: Polymorphisms in type II SH2 domain-containing inositol 5-phosphatase (INPPL1, SHIP2) are associated with physiological abnormalities of the metabolic syndrome. *Diabetes* 53:1900–1904, 2004
15. Marion E, Kaisaki PJ, Pouillon V, Gueydan C, Levy JC, Bodson A, Krzentowski G, Daubresse JC, Mockel J, Behrends J, Servais G, Szpirer C, Kruys V, Gauguier D, Schurmans S: The gene INPPL1, encoding the lipid phosphatase SHIP2, is a candidate for type 2 diabetes in rat and man. *Diabetes* 51:2012–2017, 2002
16. Pesesse X, Moreau C, Drayer AL, Woscholski R, Parker P, Erneux C: The SH2 domain containing inositol 5-phosphatase SHIP2 displays phosphatidylinositol 3,4,5-trisphosphate and inositol 1,3,4,5-tetrakisphosphate 5-phosphatase activity. *FEBS Lett* 437:301–303, 1998
17. Backers K, Blero D, Paternotte N, Zhang J, Erneux C: The termination of PI3K signalling by SHIP1 and SHIP2 inositol 5-phosphatases. *Adv Enzyme Regul* 43:15–28, 2003
18. Wada T, Sasaoka T, Funaki M, Hori H, Murakami S, Ishiki M, Haruta T, Asano T, Ogawa W, Ishihara H, Kobayashi M: Overexpression of SH2-containing inositol phosphatase 2 results in negative regulation of insulin-induced metabolic actions in 3T3–L1 adipocytes via its 5′-phosphatase catalytic activity. *Mol Cell Biol* 21:1633–1646, 2001
19. Sasaoka T, Hori H, Wada T, Ishiki M, Haruta T, Ishihara H, Kobayashi M: SH2-containing inositol phosphatase 2 negatively regulates insulin-induced glycogen synthesis in L6 myotubes. *Diabetologia* 44:1258–1267, 2001
20. Sasaoka T, Wada T, Fukui K, Murakami S, Ishihara H, Suzuki R, Tobe K, Kadowaki T, Kobayashi M: SH2-containing inositol phosphatase 2 predominantly regulates Akt2, and not Akt1, phosphorylation at the plasma membrane in response to insulin in 3T3–L1 adipocytes. *J Biol Chem* 279:14835–14843, 2004
21. Hori H, Sasaoka T, Ishihara H, Wada T, Murakami S, Ishiki M, Kobayashi M: Association of SH2-containing inositol phosphatase 2 with the insulin resistance of diabetic db/db mice. *Diabetes* 51:2387–2394, 2002
22. Murakami S, Sasaoka T, Wada T, Fukui K, Nagira K, Ishihara H, Usui I, Kobayashi M: Impact of Src homology 2-containing inositol 5′-phosphatase 2 on the regulation of insulin signaling leading to protein synthesis in 3T3–L1 adipocytes cultured with excess amino acids. *Endocrinology* 145:3215–3223, 2004
23. Michael MD, Kulkarni RN, Postic C, Previs SF, Shulman GI, Magnuson MA, Kahn CR: Loss of insulin signaling in hepatocytes leads to severe insulin resistance and progressive hepatic dysfunction. *Mol Cell* 6:87–97, 2000
24. Rutter GA: Diabetes: the importance of the liver. *Curr Biol* 10:R736–R738, 2000

25. O'Brien RM, Streeper RS, Ayala JE, Stadelmaier BT, Hornbuckle LA: Insulin-regulated gene expression. *Biochem Soc Trans* 29:552–558, 2001
26. Kubota N, Tobe K, Terauchi Y, Eto K, Yamauchi T, Suzuki R, Tsubamoto Y, Komeda K, Nakano R, Miki H, Satoh S, Sekihara H, Sciacchitano S, Lesniak M, Aizawa S, Nagai R, Kimura S, Akanuma Y, Taylor SI, Kadowaki T: Disruption of insulin receptor substrate 2 causes type 2 diabetes because of liver insulin resistance and lack of compensatory β-cell hyperplasia. *Diabetes* 49:1880–1889, 2000
27. Mithieux G, Daniele N, Payrastre B, Zitoun C: Liver microsomal glucose-6-phosphatase is competitively inhibited by the lipid products of phosphatidylinositol 3-kinase. *J Biol Chem* 273:17–19, 1998
28. Cho H, Mu J, Kim JK, Thorvaldsen JL, Chu Q, Crenshaw EB 3rd, Kaestner KH, Bartolomei MS, Shulman GI, Birnbaum MJ: Insulin resistance and a diabetes mellitus-like syndrome in mice lacking the protein kinase Akt2 (PKBβ). *Science* 292:1728–1731, 2001
29. Barthel A, Schmoll D: Novel concepts in insulin regulation of hepatic gluconeogenesis. *Am J Physiol Endocrinol Metab* 285:E685–E692, 2003
30. Matsumoto M, Ogawa W, Teshigawara K, Inoue H, Miyake K, Sakaue H, Kasuga M: Role of the insulin receptor substrate 1 and phosphatidylinositol 3-kinase signaling pathway in insulin-induced expression of sterol regulatory element–binding protein 1c and glucokinase genes in rat hepatocytes. *Diabetes* 51:1672–1680, 2002
31. Noguchi T, Matsuda T, Tomari Y, Yamada K, Imai E, Wang Z, Ikeda H, Tanaka T: The regulation of gene expression by insulin is differentially impaired in the liver of the genetically obese-hyperglycemic Wistar fatty rat. *FEBS Lett* 328:145–148, 1993
32. Shimano H, Horton JD, Hammer RE, Shimomura I, Brown MS, Goldstein JL: Overproduction of cholesterol and fatty acids causes massive liver enlargement in transgenic mice expressing truncated SREBP-1a. *J Clin Invest* 98:1575–1584, 1996
33. Beale EG, Chrapkiewicz NB, Scoble HA, Metz RJ, Quick DP, Noble RL, Donelson JE, Biemann K, Granner DK: Rat hepatic cytosolic phosphoenolpyruvate carboxykinase (GTP): structures of the protein, messenger RNA, and gene. *J Biol Chem* 260:10748–10760, 1985
34. Shingu R, Nakajima H, Horikawa Y, Hamaguchi T, Yamasaki T, Miyagawa J, Namba M, Hanafusa T, Matsuzawa Y: Expression and distribution of glucose-6-phosphatase catalytic subunit messenger RNA and its changes in the diabetic state. *Res Commun Mol Pathol Pharmacol* 93:13–24, 1996
35. Miyake K, Ogawa W, Matsumoto M, Nakamura T, Sakaue H, Kasuga M: Hyperinsulinemia, glucose intolerance, and dyslipidemia induced by acute inhibition of phosphoinositide 3-kinase signaling in the liver. *J Clin Invest* 110:1483–1491, 2002
36. Jaffe HA, Danel C, Longenecker G, Metzger M, Setoguchi Y, Rosenfeld MA, Gant TW, Thorgeirsson SS, Stratford-Perricaudet LD, Perricaudet M, Pavirani A, Lecocq JP, Crystal RG: Adenovirus-mediated in vivo gene transfer and expression in normal rat liver. *Nat Genet* 1:372–378, 1992
37. Alessi DR, Andjelkovic M, Caudwell B, Cron P, Morrice N, Cohen P, Hemmings BA: Mechanism of activation of protein kinase B by insulin and IGF-1. *EMBO J* 15:6541–6551, 1996
38. Andjelkovic M, Alessi DR, Meier R, Fernandez A, Lamb NJC, Frech M, Cron P, Cohen P, Lucocq JM, Hemmings BA: Role of translocation in the activation and function of protein kinase B. *J Biol Chem* 272:31515–31524, 1997
39. Kobayashi K, Forte TM, Taniguchi S, Ishida BY, Oka K, Chan L: The db/db mouse, a model for diabetic dyslipidemia: molecular characterization and effects of Western diet feeding. *Metabolism* 49:22–31, 2000
40. Shao J, Yamashita H, Qiao L, Friedman JE: Decreased Akt kinase activity and insulin resistance in C57BL/KsJ-Lepr$^{db/db}$ mice. *J Endocrinol* 167:107–115, 2000
41. Sleeman MW, Wortley KE, Lai KM, Gowen LC, Kintner J, Kline WO, Garcia K, Stitt TN, Yancopoulos GD, Wiegand SJ, Glass DJ: Absence of the lipid phosphatase SHIP2 confers resistance to dietary obesity. *Nat Med* 11:199–205, 2005
42. Maehama T, Dixon JE: The tumor suppressor, PTEN/MMAC1, dephosphorylates the lipid second messenger, phosphatidylinositol 3,4,5-trisphosphate. *J Biol Chem* 273:13375–13378, 1998
43. Stiles B, Wang Y, Stahl A, Bassilian S, Lee WP, Kim YJ, Sherwin R, Devaskar S, Lesche R, Magnuson MA, Wu H: Liver-specific deletion of negative regulator Pten results in fatty liver and insulin hypersensitivity. *Proc Natl Acad Sci U S A* 101:2082–2087, 2004
44. Butler M, McKay RA, Popoff IJ, Gaarde WA, Witchell D, Murray SF, Dean NM, Bhanot S, Monia BP: Specific inhibition of PTEN expression reverses hyperglycemia in diabetic mice. *Diabetes* 51:1028–1034, 2002
45. Postic C, Shiota M, Magnuson MA: Cell-specific roles of glucokinase in glucose homeostasis. *Recent Prog Horm Res* 56:195–217, 2001
46. Horton JD, Shimomura I, Ikemoto S, Bashmakov Y, Hammer RE: Overexpression of sterol regulatory element-binding protein-1a in mouse adipose tissue produces adipocyte hypertrophy, increased fatty acid secretion, and fatty liver. *J Biol Chem* 278:36652–36660, 2003
47. Vuguin P, Raab E, Liu B, Barzilai N, Simmons R: Hepatic insulin resistance precedes the development of diabetes in a model of intrauterine growth retardation. *Diabetes* 53:2617–2622, 2004
48. Shimomura I, Matsuda M, Hammer RE, Bashmakov Y, Brown MS, Goldstein JL: Decreased IRS-2 and increased SREBP-1c lead to mixed insulin resistance and sensitivity in livers of lipodystrophic and ob/ob mice. *Mol Cell* 6:77–86, 2000
49. Seoane J, Trinh K, O'Doherty RM, Gómez-Foix AM, Lange AJ, Newgard CB, Guinovart JJ: Metabolic impact of adenovirus-mediated overexpression of the glucose-6-phosphatase catalytic subunit in hepatocytes. *J Biol Chem* 272:26972–26977, 1997
50. Sun Y, Liu S, Ferguson S, Wang L, Klepcyk P, Yun JS, Friedman JE: Phosphoenolpyruvate carboxykinase overexpression selectively attenuates insulin signaling and hepatic insulin sensitivity in transgenic mice. *J Biol Chem* 277:23301–23307, 2002

GLIA 52:47–52 (2005)

Evidence for Creatine Biosynthesis in Müller Glia

TOSHIHISA NAKASHIMA,[1] MASATOSHI TOMI,[1] MASANORI TACHIKAWA,[2] MASAHIKO WATANABE,[3] TETSUYA TERASAKI,[2,4,5] AND KEN-ICHI HOSOYA[1]*
[1]*Faculty of Pharmaceutical Sciences, Toyama Medical and Pharmaceutical University, Toyama, Japan*
[2]*Department of Molecular Biopharmacy and Genetics, Graduate School of Pharmaceutical Sciences, Tohoku University, Sendai, Japan*
[3]*Department of Anatomy, Hokkaido University School of Medicine, Sapporo, Japan*
[4]*New Industry Creation Hatchery Center, Tohoku University, Sendai, Japan*
[5]*SORST of the Japan Science and Technology Agency (JST), Kawaguchi, Saitama, Japan*

KEY WORDS
GAMT; rat retina; immunohistochemistry; glutamine synthetase; Müller cell line

ABSTRACT
In high-energy metabolic tissues like the retina, creatine may play an important role in energy storage and in transmission of phosphate-bound energy substrates. To prove this, we investigated creatine synthesis in Müller glia. We also characterized the localization of the creatine synthetic enzyme, S-adenosyl-L-methionine:N-guanidinoacetate methyltransferase (GAMT) in the retina. Reverse transcription-polymerase chain reaction analysis revealed that L-arginine:glycine amidinotransferase and GAMT mRNAs were expressed in the retina and the Müller cell line, TR-MUL5. [^{14}C]Creatine was detected after incubation of isolated rat retina or TR-MUL5 cells with [^{14}C]glycine, L-arginine and L-methionine, suggesting creatine synthesis in Müller glia. Western blot analysis also revealed expression of GAMT protein in the rat retina and TR-MUL5 cells. Furthermore, confocal immunofluorescent microscopy of dual-labeled rat retinal sections demonstrated co-localization of GAMT with glutamine synthetase. Taken together, the results of the present study indicate creatine synthesis in Müller glia, implying an important role of creatine in energy metabolism in the retina.

INTRODUCTION

The creatine/phosphocreatine system plays a pivotal role in the maintenance of ATP homeostasis in highly energy-demanding tissues such as the brain and skeletal muscles (Wyss and Kaddurah-Daouk, 2000). High levels of creatine in the chick retina (3 mM) and in the photoreceptor cells (10–15 mM) suggest that the creatine/phosphocreatine system may also be significant in the retina, where photoreceptor cells require a large amount of metabolic energy for phototransduction maintained by ionic gradients across the plasma membrane (Hall and Kühn, 1986; Wallimann et al., 1986; Sather and Detwiler, 1987). In fact, it has been shown that the gyrate atrophy (GA) of the choroids and retina is characterized by hyperornithinemia and hypocreatinemia, implying that excessive ornithine leads to chorioretinal degeneration through suspension of creatine synthesis (Sipila et al., 1992). The high level of creatine in the retina is maintained by a supply from the circulating blood through the blood-retinal barrier (BRB) or local biosynthesis in the retina. We have recently shown the presence of a creatine transporter (CRT) at the rat inner blood-retinal barrier (inner BRB) (Nakashima et al., 2004). A deficiency of creatine transporters in humans results in mental retardation, seizures and central hypotonia (Schulze, 2003). However, retinal dysfunction or degeneration rarely develops in these patients, suggesting that transportation of creatine from the circulating blood does not play an important role in sustaining the creatine/phosphocreatine system in the retina. We now hypothesize that creatine can be synthesized locally in the retina. Although creatine is mainly synthesized in other organs, such as the kidney, liver, and pancreas, creatine is also synthesized in the brain (Defalco and Davies, 1961; Wyss and Kaddurah-Daouk, 2000). In the central nervous system, it has been shown that S-adenosyl-L-methionine:N-guanidinoacetate methyltransferase (GAMT), a key enzyme for creatine synthesis, is highly and exclusively expressed in glial cells, including oligodendrocytes, olfactory ensheathing glia, and astrocytes, raising the possibility that creatine is also synthesized in Müller glia, the most predominant glia in the retina (Dringen et al., 1998; Tachikawa et al., 2004). Although GAMT activities have been demonstrated in the retina of various species including rats, there have been no investigations of the cellular system for creatine biosynthesis in the retina (Mardashchev, 1975). Using high-performance liquid chromatography (HPLC), reverse transcription-polymerase chain reaction (RT-PCR), Western blot analysis, and confocal immunofluorescence imaging, we report that creatine is synthesized in Müller glia.

Grant sponsor: Japan Society for the Promotion of Science; Grant sponsor: Ministry of Health, Labor, and Welfare, Japan.

Masanori Tachikawa is currently at the Faculty of Pharmaceutical Sciences, Toyama Medical and Pharmaceutical University, Toyama, Japan.

*Correspondence to: Ken-ichi Hosoya, Faculty of Pharmaceutical Sciences, Toyama Medical and Pharmaceutical University, 2630 Sugitani, Toyama 930-0194, Japan. E-mail: hosoyak@ms.toyama-mpu.ac.jp

Received 8 November 2004; Accepted 7 March 2005

DOI 10.1002/glia.20222

Published online 12 May 2005 in Wiley InterScience (www.interscience.wiley.com).

MATERIALS AND METHODS

Animals

Male Wistar rats (250–300 g), male ddY mice (25–30 g), and female New Zealand White rabbits (3.1–3.5 kg) were purchased from SLC (Shizuoka, Japan). The investigations using animals described in this report conformed to the provisions of the Animal Care Committee, Toyama Medical and Pharmaceutical University (#2003-48), and the ARVO Statement on the Use of Animals in Ophthalmic and Vision Research.

Reagents

[1-^{14}C]D-Mannitol ([^{14}C]D-mannitol, 53.7 mCi/mmol), and [U-^{14}C]glycine ([^{14}C]glycine, 101 mCi/mmol) were purchased from Amersham Biosciences (Buckinghamshire, UK); L-[2,3,4-^{3}H] L-arginine HCl ([^{3}H] L-arginine, 40 Ci/mmol) was from Perkin-Elmer Life Sciences (Boston, MA); [4-^{14}C]creatine ([^{14}C]creatine, 55 mCi/mmol) was from American Radiolabeled Chemicals (St. Louis, MO). All other chemicals were of reagent grade and available commercially.

Cell Culture

TR-MUL5 cells, which had been established and characterized previously (Tomi et al., 2003), were used as an in vitro model of Müller glia to examine expression of creatine biosynthetic enzymes and biosynthesis of creatine. TR-MUL5 cells (passages 15–25) were cultured at 33°C in Dulbecco's modified Eagle's medium (Nissui Pharmaceuticals, Tokyo, Japan) under 5% CO_2/air. The permissive temperature for the culture of TR-MUL5 cells is 33°C, due to the expression of temperature-sensitive large T-antigen (Tomi et al., 2003; Hosoya and Tomi, 2005). For the biosynthesis and uptake studies, cells (3×10^5 cells/cm^2) were cultured at 33°C for 24 h on a 24-well tissue culture plate (BD Biosciences, Bedford, MA).

An Ex Vivo Rat Retinal Preparation

Retinal isolation and ex vivo studies were performed using a modification of the procedure described by Izumi et al. (1995). Briefly, under deep pentobarbital anesthesia (100 mg/kg body weight, i.p.), the eyes of Wistar rats were enucleated, and retinas were dissected in ice-cold phosphate-buffered saline (PBS). Freshly extirpated retinas were placed on the insert of a Transwell^{TM} (12-mm diameter, 0.4-μm pore size, polycarbonate membranes) (Corning, New York, NY) and pre-incubated in 1 ml minimal medium (MM; 110 mM NaCl, 44 mM $NaHCO_3$, 1.8 mM $CaCl_2$, 5.4 mM KCl, 0.8 mM $MgSO_4$, 0.92 mM NaH_2PO_4, containing 10% dialyzed fetal bovine serum, 1 mM L-methionine, and 1 mM L-arginine, pH 7.4) (Dringen et al., 1998), which was equilibrated with 5% CO_2/95% O_2, at 30°C for 1 h.

Creatine Biosynthesis Study

After pre-incubation of isolated retinas, the inserts were transferred to other wells and were incubated in 1 ml MM containing 1 μCi [^{14}C]glycine (10 μM) at 37°C in dark and a humidified atmosphere of 5% CO_2/air for 24 h. TR-MUL5 cells were washed three times with 1 ml MM and then incubated in 1 ml MM containing 1 μCi [^{14}C]glycine (10 μM) at 33°C in a humidified atmosphere of 5% CO_2/air for 24 h. After a 24 h-incubation, retinas and cells were washed with ice-cold PBS and homogenized in ice-cold 70% methanol. After centrifugation at 4°C and 12,000*g* for 5 min, an aliquot of the samples was subjected to HPLC using a system equipped with a 4.6 × 150-mm Inertsil ODS-3 column (GL Sciences, Tokyo, Japan). The mobile phase consisted of 99.5% 5 mM 1-octanesulfonic acid and 30 mM K_2HPO_4–0.5% methanol (pH 2.5) at a flow rate of 0.5 ml/min. The eluent was collected in vials, and the radioactivity in each fraction was determined by liquid scintillation counting.

RT-PCR Analysis

Total cellular RNA was prepared from PBS-washed cells using the RNeasy Mini Kit (Qiagen, Hilden, Germany). Single-strand cDNA was made from 1 μg total RNA by reverse transcription (RT) using oligo dT primer. The polymerase chain reaction (PCR) was performed using a gene amplification system (GeneAmp PCR system 9700; PE-Applied Biosystems, Foster City, CA) with GAMT and L-arginine:glycine amidinotransferase (AGAT) through 40 cycles of 94°C for 30 s, 62°C for 1 min, and 72°C for 2 min. The sequences of the specific primers were as follows: sense, 5′-TCT GAC ACG CAC CTG CAG ATC C-3′; antisense, 5′-GCA TAG TAG CGG CAG TCG GCT G-3′ for rat GAMT (GenBank accession number X08056); sense, 5′-TAA CAG GAT GGG TGC AGC GAA CT-3′; antisense, 5′-GGT CAT ACA GTT CGT CAG CCA T-3′ for rat arginine/glycine aminotransferase (AGAT) (GenBank accession number U07971). The PCR products were separated by electrophoresis on an agarose gel in the presence of ethidium bromide and visualized under ultraviolet (UV) light. The molecular identity of the resultant product was confirmed by sequence analysis using a DNA sequencer (Prism 310; PE-Applied Biosystems).

Western Blot Analysis

Tissue and cell lysates of adult mouse brain, adult rat brain, retina, liver, and TR-MUL5 cells were prepared in sample buffer consisting of 5% sodium dodecyl sulfate (SDS), 50 mM Tris-HCl (pH 6.8), 10% glycerol, 6% 2-mercaptoethanol, 0.01% bromophenol blue, and 0.1% protease-inhibitor cocktail (Sigma, St. Louis, MO). To prepare total protein fractions, the lysates were centrifuged at 8,000 g and 4°C for 10 min, and the super-

natants were collected. The protein concentration was measured using a kit (DC, Bio-Rad, Hercules, CA). The protein was electrophoresed on a 12% SDS-polyacrylamide gel and electrotransferred to a polyvinylidene difluoride (PVDF) membrane (Bio-Rad). The blotted membranes were incubated with affinity-purified guinea pig polyclonal antibody against mouse GAMT (Tachikawa et al., 2004) at 1.5 μg/ml as the primary antibody using blocking agent solution (Block Ace; Dainihon Pharmaceutical, Osaka, Japan). There was apparently sufficient antibody cross-reactivity between mouse and rat GAMT (Fig. 3). The membranes were subsequently incubated with horseradish peroxidase conjugated donkey anti-guinea pig IgG antibody as the secondary antibody. The bands were visualized with an enhanced chemiluminescence kit (ECL; Amersham Biosciences).

Immunohistochemistry

Under deep pentobarbital anesthesia, Wistar rats were perfused transcardially with 4% paraformaldehyde in 0.1 M sodium phosphate buffer (pH 7.2). The retina was embedded in paraffin wax after dehydration using graded alcohols, and paraffin sections (5-μm thickness) were prepared with a sliding microtome (SM2000R; Leica Microsystems, Wetzlar, Germany). Before immunohistochemical investigation, the paraffin sections were digested with pepsin (1 mg/ml in 0.2 M HCl, Dako, Carpinteria, CA) for 5 min at 37°C to retrieve antigens. For immunofluorescence, sections were incubated at room temperature with 10% normal goat serum (NGS) for 30 min, guinea pig anti-GAMT antibody 2 μg/ml singly or in combination with rabbit anti-glutamine synthetase antibody (1 μg/ml) overnight, and subsequently incubated with FITC- or Cy3-conjugated secondary antibodies for 2 h (Jackson ImmunoResearch, West Grove, PA). Polyclonal antibody to glutamine synthetase (GS) was raised against amino acid residues 344–373 of mouse GS (GenBank accession number AY044241). The polypeptides were synthesized and linked to maleimide-activated keyhole limpet hemocyanin (KLH; Pierce, Rockford, IL). The KLH-linked polypeptides (200 μg/injection) were emulsified by mixing with an equal volume of Freund's adjuvant (Difco, Detroit, MI) and injected subcutaneously into female New Zealand White rabbits at intervals of 2 weeks. Two weeks after the sixth injection, affinity-purified antibodies were prepared, first using protein G-Sepharose (Amersham Biosciences) and then using antigen polypeptides free of KLH coupled to cyanogen bromide-activated Sepharose 4B (Amersham Biosciences). Western blot analysis using mouse brain, rat brain, and rat retina extracts showed that rabbit anti-GS antibody strongly recognized a single protein band at 44 kDa (data not shown), the size of which is consistent with that of a previous report (Shen et al., 2004). Photographs were taken with a confocal laser scanning microscope (Fluoview, Olympus, Tokyo, Japan).

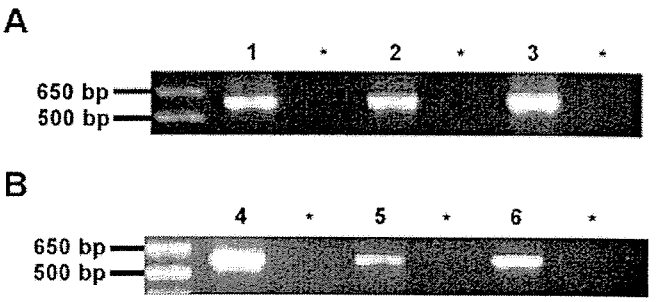

Fig. 1. Reverse transcription-polymerase chain reaction (RT-PCR) analysis of GAMT (**A**) and AGAT (**B**) in the rat retina and TR-MUL5 cells. **Lane 1**, rat liver; **lanes 2 and 5**, rat retina; **lanes 3 and 6**, TR-MUL5 cells; **lane 4**, rat brain; asterisk, in the absence of reverse transcriptase for the respective left-hand lane. Rat liver and brain were used as a positive control for GAMT and AGAT, respectively.

RESULTS

Expression of GAMT and AGAT mRNAs in the Rat Retina and TR-MUL5 Cells

To examine the expression of creatine biosynthetic enzymes in the retina and Müller glia, we performed RT-PCR analysis, using total RNA isolated from the rat retina and Müller cell line, TR-MUL5, and specific primers for rat GAMT and AGAT (Fig. 1). Using the rat liver (lane 1) and brain (lane 4) as positive controls, GAMT and AGAT cDNAs were successfully amplified at 584 and 591 bp, respectively, in the retina (lanes 2 and 5) and TR-MUL5 cells (lanes 3 and 6). These results indicate that creatine biosynthetic enzymes are transcribed in the rat retina and TR-MUL5 cells.

Creatine Biosynthesis in the Rat Retina and TR-MUL5 Cells

Creatine is synthesized from glycine and -L-arginine, and two carbons of creatine are derived from glycine. Thus, we used [^{14}C]glycine to determine whether creatine is biosynthesized by detecting [^{14}C]creatine using HPLC. Firstly, the uptake of [^{14}C]glycine and [^{3}H]-L-arginine by TR-MUL5 cells was examined. The initial uptake rate of [^{14}C]glycine and [^{3}H]L-arginine in TR-MUL5 cells was 7.29 μl/(min · mg protein) and 28.3 μl/(min · mg protein), which were 14.5-fold and 56.4-fold greater, respectively, than that of [^{3}H]-D-mannitol (0.502 μl/(min · g protein)) (data not shown). This finding suggests that the precursor amino acids, glycine and L-arginine, are taken up by TR-MUL5 cells at much greater rates than by nonspecific adsorption or passive diffusion.

Figure 2 shows the HPLC chromatograms of [^{14}C]glycine (Fig. 2A), [^{14}C]creatine (Fig. 2B), and samples of isolated retina (Fig. 2C) and TR-MUL5 cells (Fig. 2D). After 24-h incubation of isolated retinas and TR-MUL5 cells with [^{14}C]glycine, the peaks of [^{14}C]creatine appeared at the same time point both in isolated retina

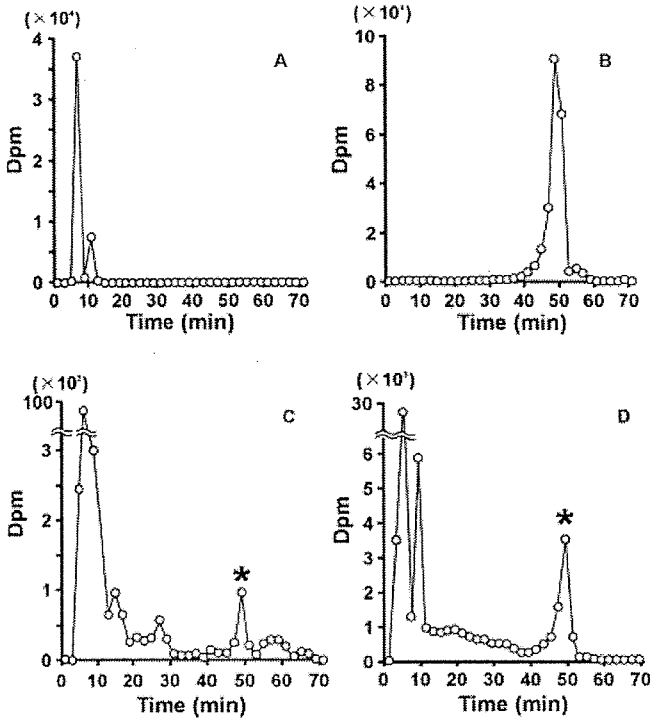

Fig. 2. Typical high-performance liquid chromatography (HPLC) of samples of isolated rat retina (**C**) and TR-MUL5 cells (**D**). The isolated retinas and TR-MUL5 cells were incubated in medium containing 1 μCi [^{14}C]glycine (10 μM), L-arginine (1 mM), and L-methionine (1 mM) for 24 h at 37 and 33°C, respectively. The asterisk indicates [^{14}C]-labeled creatine synthesized from [^{14}C]glycine in the rat retinas and TR-MUL5 cells. **A,B:** Typical chromatograms of [^{14}C]glycine and [^{14}C]creatine, respectively.

(Fig. 2C) and TR-MUL5 cells (Fig. 2D), suggesting creatine biosynthesis in the rat retina and Müller glia.

Preferential Distribution of GAMT in Müller Glia of the Rat Retina

We then examined the distribution of GAMT in the rat retina by confocal immunofluorescence microscopy. Although anti-GAMT antibody was raised against amino acids residues 1–236 of mouse GAMT (Tachikawa et al., 2004), sufficient cross-reactivity between mouse and rat was found by Western blot analysis (Fig. 3). Similarly to the mouse brain (lane 1), rat liver (lane 2), and rat brain (lane 3), a band at 27 kDa was observed in the rat retina (lane 4) and TR-MUL5 cells (lane 5).

Using double immunofluorescence, intense GAMT immunoreactivity was found to be distributed in fibrous structures, which projected radially throughout the retina from the inner to the outer limiting membrane (Fig. 4A). The fibrous structures extensively overlapped with GS, a specific marker for glial cells in the retina (Fig. 4B–D). GAMT was also detected in GS-positive Müller cell bodies (Fig. 4C, arrowheads), and Müller cells and astrocytes in the ganglion cell layer (Fig. 4D). In addition, tiny puncta with low to moderate GAMT

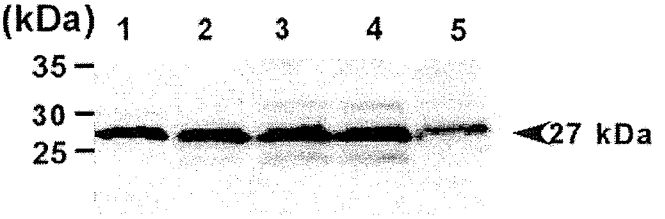

Fig. 3. Western blot analysis of rat GAMT using anti-mouse GAMT antibody in the rat retina and TR-MUL5 cells. **Lane 1**, mouse brain; **lane 2**, rat liver; **lane 3**, rat brain; **lane 4**, rat retina; **lane 5**, TR-MUL5 cells. The single band at 27 kDa in the rat retina and TR-MUL5 cells has the same molecular weight as that in the mouse brain, rat liver, and rat brain used as positive controls.

intensity were also detected between the fibrous structures, but they were negative for glutamine synthetase (Figs. 4B-D). Such characteristic immunostaining was abolished when preimmune guinea pig immunoglobulin or primary antibody preabsorbed with GAMT antigen peptides (100 μg/ml; data not shown) was used. These features indicate that GAMT is exclusively expressed in Müller glia with additional expression in neuronal cells or some other glial cells at low to moderate levels.

DISCUSSION

The present study demonstrates the expression of creatine biosynthetic enzymes and creatine biosynthesis in the rat retina and TR-MUL5 cells. Moreover, there is preferential localization of GAMT in Müller cells of the rat retina. This is the first direct evidence of creatine biosynthesis in Müller cells of the retina.

Glycine and L-arginine, which are precursor amino acids for creatine biosynthesis, are thought to be synthesized de novo in the cells. However, there is no report regarding de novo synthesis of both amino acids in Müller cells. In TR-MUL5 cells, uptake rate of glycine and L-arginine was much faster than that of D-mannitol, suggesting that some neutral and cationic amino acid transporters actively transport these amino acids. This evidence is consistent with previous reports (Pow and Crook, 1997; Gadea et al., 1999; Reye et al., 2001). Glycine transport appears to take place via Glyt-1 and/or system A in the primary cultured Müller cells (Gadea et al., 1999; Reye et al., 2001). L-Arginine transport may occur in retinal Müller glia (Pow and Crook, 1997). In contrast, Reye et al. (2001) reported that Glyt-1 is not expressed in Müller glia in vivo. The lack of agreement between the expression of glycine transporter in the cultured Müller cells and Müller glia in vivo needs an explanation. Conceivably, Glyt-1 is up-regulated in cultured Müller cells. Although further studies are needed to identify glycine and L-arginine transporters in Müller glia in vivo, TR-MUL5 cells have the ability to take up glycine and L-arginine. The expression of AGAT and GAMT mRNA in the retina and TR-MUL5 cells suggests that creatine biosynthesis takes place in Müller glia (Fig. 1).

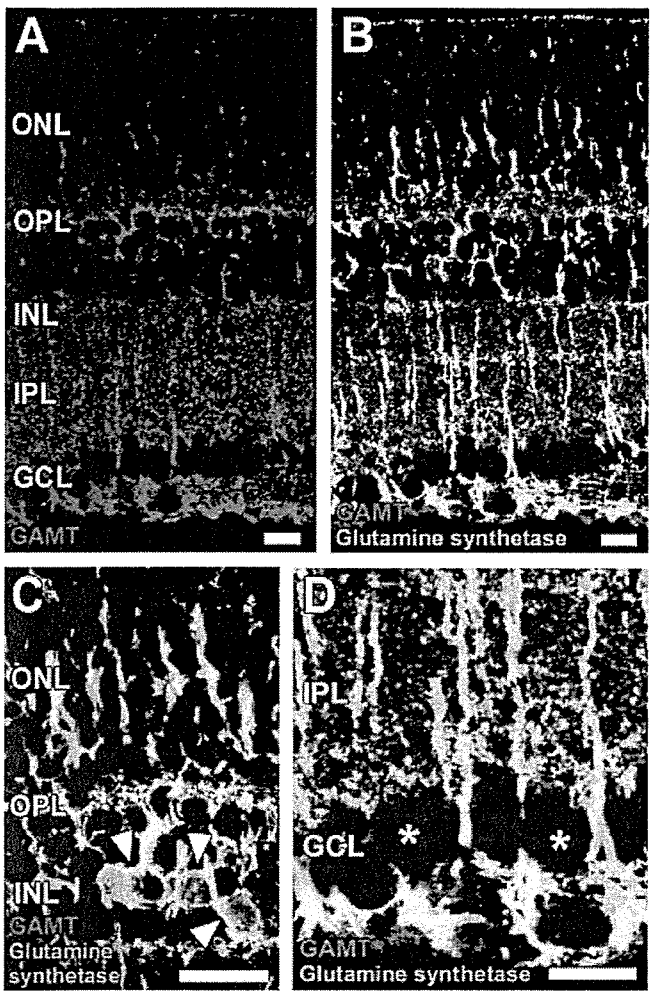

Fig. 4. Confocal immunofluorescence microscope images of single (**A**) or dual-labeled (**B–D**) rat retinal sections. The retinal sections were stained with anti-GAMT antibody (red) singly (A) or in combination with anti-glutamine synthetase antibody (green), a marker for glial cells (B–D). Arrowheads (C) and asterisks (D) indicate Müller cell bodies and ganglion cell bodies, respectively. ONL, outer nuclear layer; OPL, outer plexiform layer; INL, inner nuclear layer; IPL, inner plexiform layer; GCL, ganglion cell layer. Scale bars = 10 μm.

Indeed, [^{14}C]creatine was identified in the isolated retina and TR-MUL5 cells after a 24 h-incubation with [^{14}C]glycine added to the culture medium (Fig. 2). Moreover, confocal immunofluorescence microscopy with rat retinal sections demonstrated that GAMT is preferentially localized in GS-positive retinal cells, i.e., Müller cells and astrocytes (Fig. 4). Astrocytes are largely confined to the nerve fiber layer of the retina (Pfeiffer-Guglielmi et al., 2004) and GS-positive cells are mainly seen in profile, with their endfeet within the nerve fiber layer and their cell bodies in the inner nuclear layer (Fig. 4). These features suggest that creatine biosynthesis is mainly responsible for Müller cells and partly for astrocytes in the rat retina. These findings support the hypothesis that creatine is largely biosynthesized in Müller glia.

The role and fate of creatine synthesized in retinal Müller cells remain unknown. We assume that synthesized creatine is not only used by Müller cells, but is also supplied to other cells, most likely photoreceptor cells, to maintain ATP homeostasis. Visual transduction processes in photoreceptor cells involve many ATP-requiring reactions, such as ATP-dependent regeneration and phosphorylation of the rhodopsin photopigment by rhodopsin kinase, ATP-dependent Na^+, K^+-ATPase of the photoreceptor cell membrane, ATP-dependent phosphotidylinositol/inositol trisphosphate-signaling pathway, and ATP-requiring neurotransmitter synthesis (Koenekoop, 2004). To meet this enormous requirement, photoreceptor cells are thought to generate 34 ATP via the tricarboxylic acid (TCA) cycle rather than from glycolysis using 2 molecules of lactate supplied from local Müller glia (Poitry-Yamate et al., 1995; Magistretti et al., 1999). Since the rate of ATP generation by the creatine/phosphocreatine shuttle system is 10-fold faster than that by oxidative phosphorylation and glycolysis (Wallimann et al., 1992), the creatine/phosphocreatine shuttle system may play a pivotal role in energy storage and regeneration of ATP in photoreceptor cells. In support of this notion, the creatine concentration in chicken photoreceptor cells is as high as 10–15 mM (Wallimann et al., 1986). Interestingly, as far as this point is concerned, creatine kinases are also more concentrated in photoreceptor cells compared with other cells in the chicken retina (Wallimann et al., 1986). Despite the abundance of creatine and creatine kinases, we observed little GAMT immunoreactivity in photoreceptor cells located in the outer nuclear layer, but, instead, intense GAMT immunoreactivity in GS-positive Müller cells (Fig. 4). Therefore, it appears likely that creatine enriched in photoreceptor cells is derived, at least in part, from local Müller glia, like lactate and amino acids which are assumed to be shuttled between Müller cells and photoreceptor cells (Poitry-Yamate et al., 1995; Rauen and Wiessner, 2000). Bearing in mind the fact that creatine is also supplied from the circulating blood via CRT at the inner BRB (Nakashima et al., 2004), the creatine concentration in photoreceptor cells may be controlled by a dual system of creatine supply, i.e., supplies from the local retinal glial cells and capillaries. As far as this novel idea is concerned, there is no report of retinal dysfunction in patients with CRT deficiency. However, it can be explained by creatine synthesis and supply by Müller glia. In contrast, chorioretinal degeneration in patients with GA can be ascribed both to a reduced creatine supply from the circulating blood and a disrupted supply from local Müller glia due to inhibition of creatine biosynthesis by hyperornithinemia in the whole body (Sipila et al., 1980).

The creatine uptake system in photoreceptor cells has not yet been identified. Jones (1995) reported identification and localization of CRT in bovine retina by in situ hybridization showing that CRT mRNA was expressed in all cell types in the retina, whereas CRT mRNA was absent in photoreceptor cells. Although further studies are needed to identify the creatine transport system(s)